Bulk viscosity from Urca processes: *npeμ* matter in the neutrino-trapped regime

Mark Alford[*]
Department of Physics, Washington University, St. Louis, Missouri 63130, USA

Arus Harutyunyan[†]
Byurakan Astrophysical Observatory, Byurakan 0213, Armenia and Department of Physics, Yerevan State University, Yerevan 0025, Armenia

Armen Sedrakian[‡]
Frankfurt Institute for Advanced Studies, D-60438 Frankfurt am Main, Germany and Institute of Theoretical Physics, University of Wrocław, 50-204 Wrocław, Poland

(Received 27 August 2021; accepted 5 October 2021; published 18 November 2021)

In this work, we extend our previous study of the bulk viscosity of hot and dense npe matter induced by the Urca processes in the neutrino trapped regime to $npe\mu$ matter by adding the muonic Urca processes as well as the purely leptonic electroweak processes involving electron-muon transition. The nuclear matter is modeled in a relativistic density functional approach with two different parametrizations which predict neutrino dominated matter (DDME2 model) and antineutrino dominated matter (NL3 model) at temperatures for which neutrinos/antineutrinos are trapped. In the case of neutrino-dominated matter, the main equilibration mechanism is lepton capture, whereas in the case of antineutrino-dominated matter this is due to neutron decay. We find that the equilibration rates of Urca processes are higher than that of the pure leptonic processes, which implies that the Urca-process-driven bulk viscosity can be computed with the leptonic reactions assumed to be frozen. We find that the bulk viscosity decreases with temperature as $\zeta \sim T^{-2}$ at moderate temperatures. At high temperatures this scaling breaks down by sharp drops of the bulk viscosity close to the temperature where the proton fraction is density-independent and the matter becomes scale-invariant. This occurs also when the matter undergoes a transition from the antineutrino-dominated regime to the neutrino-dominated regime where the bulk viscosity attains a local maximum. We also estimate the bulk viscous dissipation timescales and find that these are in the range $\gtrsim 1$ s for temperatures above the neutrino trapping temperature. These timescales would be relevant only for long-lived objects formed in binary neutron star mergers and hot proto-neutron stars formed in core-collapse supernovas.

DOI: 10.1103/PhysRevD.104.103027

I. INTRODUCTION

Binary neutron star mergers, which were observed in gravitational waves by the LIGO-Virgo collaboration, offer a new setting in which to study the properties of superdense, strongly interacting matter. These events are complementary to the studies of cold neutron stars, which probe the near zero-temperature limit and heavy-ion collisions which are covering less baryon-dense finite systems. Thus, they offer an opportunity to gain insight into the physics of hot, dense and highly isospin asymmetric matter by analyzing the premerger gravitational waves (already observed in two merger events, GW170817 and GW190425 [1,2]) and the postmerger signal which will be accessible to advanced LIGO and the next-generation gravitational-wave observatories, such as the Einstein Telescope [3] and the Cosmic Explorer [4]. Furthermore, electromagnetic counterparts of the gravitational waves produced in neutron star mergers can be used to set bounds on the properties of compact stars.

Numerical simulations of neutron star mergers using the nondissipative hydrodynamics [5–16] (for reviews see [17–19]) show that the matter in the postmerger object undergoes oscillations which may be damped by dissipative processes. The initial estimates of the potential impact of dissipation on these oscillations based on cold-matter transport in neutron stars [20] highlighted the potential importance of bulk viscosity in damping the modes. Subsequent studies computed the bulk viscosity of dense matter in various regimes [21–23]. In particular, our previous work [22], focused on the neutrino-trapped regime and computed the bulk viscosity of hot nuclear matter using

[*]alford@physics.wustl.edu
[†]arus@bao.sci.am
[‡]sedrakian@fias.uni-frankfurt.de

 © 2021 American Physical Society

the relativistic density functional method for the equation of state (EoS) and single-particle spectra of baryons consistent with the prevailing conditions in the post-merger object. It was found that in the regime where neutrinos are trapped the bulk viscosity is reduced compared to the neutrino free-streaming regime. Our estimates of the damping timescales [24] indicate that the bulk viscous damping would be most efficient close the temperatures $T_{\rm tr} \sim 5$ MeV [25,26] at which the transition from trapped to the free-streaming neutrino regime occurs. The efficacy of the bulk viscosity was estimated by embedding it in the ideal hydrodynamics simulations [27], but this study was restricted to the free-streaming regime only.

The aim of this work is twofold. First, we extend our previous study [22] of neutron-proton-electron (npe) matter to include muons. It is well established that muons appear in significant amounts slightly above the nuclear saturation density, which makes their proper treatment mandatory. Their appearance gives rise to new types of Urca processes and opens up the possibility of purely leptonic electroweak processes. Thus, it is the purpose of this work to assess the impact of these processes on the bulk viscosity of $npe\mu$ matter. The second purpose of this work is to improve on the approximations used in Ref. [22], by computing the reactions rates of baryonic Urca processes in a fully relativistic manner. We show below that using relativistic rather than approximate nonrelativistic forms of baryon spectra produces a sizeable effect already above twice the nuclear saturation density. Below we focus again on the neutrino-trapped regime, in which neutrinos have a mean free path that is significantly shorter than the stellar size. The resulting nonzero lepton chemical potential affects both the composition of matter and the reaction rates, and constitutes the main difference between this work and the extensively studied low-temperature limit of npe and $npe\mu$ compositions [28–37]. We demonstrate explicitly how the low-temperature expressions are obtained from their more general counterparts derived here in Appendix A. As in Ref. [22] we will assume that thermal conduction is efficient enough to keep matter isothermal as it undergoes oscillations. While such assumption is needed for the treatment of the oscillations, the rates of various weak processes we compute below are local quantities and do not require such an assumption. The background matter will be treated within the covariant density functional models based on the DDME2 parametrization [38] with density-dependent couplings and NL3 parametrization [39] which features density-independent couplings but is supplemented with nonlinear self-interaction terms for scalar mesons. More details on these models are given in Ref. [22].

Our study is focused on the bulk viscosity, but the methods and results are of more general interest, as they can be applied to obtain other microphysical characteristic of dense matter, for example, neutrino opacities.

The density-temperature regime studied here occurs in neutron star mergers and also in supernovae and proto-neutron stars, albeit in those cases the lepton fraction is larger ($Y_e \simeq 0.4$) than in the merger case ($Y_e \simeq 0.1$) [40–42]. It is worthwhile to note that the importance of muons has been addressed recently in the supernova context as well [43,44].

This paper is organized as follows. In Sec. II we discuss the rates of the nucleonic Urca and purely leptonic processes. Section III derives the corresponding expressions for the bulk viscosity. In Sec. IV we present the results of numerical evaluation of the rates and bulk viscosity on the basis of two density functional theory models at a finite temperature which account for a neutrino component with nonzero chemical potential. Our conclusions are given in Sec. V. Appendix A details the computation of the phase-space integrals needed to evaluate the rates of the Urca processes. Finally, Appendix B details the computation of the susceptibilities of nucleonic matter, which are required for the evaluation of the bulk viscosity coefficient.

In this work we use natural (Gaussian) units with $\hbar = c = k_B = 1$, and the metric $g_{\mu\nu} = \mathrm{diag}(1, -1, -1, -1)$.

II. WEAK PROCESSES IN NEUTRON STAR MATTER

We consider neutron-star matter composed of neutrons, protons, electrons, muons, and electron and muon neutrinos in the density range $0.5n_0 \le n_B \le 5n_0$, where $n_0 \simeq 0.152$ fm^{-3} is the nuclear saturation density, and temperature range $T_{\rm tr} \le T \simeq 100$ MeV with $T_{\rm tr} \simeq 5$ MeV being the temperature above which neutrinos (or antineutrinos) are trapped in a neutron star [26].

The β-equilibration processes among the baryons we consider below are the direct Urca processes

$$n \rightleftarrows p + e^- + \bar{\nu}_e \quad (\text{neutron e} - \text{decay}), \tag{1}$$

$$p + e^- \rightleftarrows n + \nu_e \quad (\text{electron capture}), \tag{2}$$

$$n \rightleftarrows p + \mu^- + \bar{\nu}_\mu \quad (\text{neutron}\,\mu - \text{decay}), \tag{3}$$

$$p + \mu^- \rightleftarrows n + \nu_\mu \quad (\text{muon capture}). \tag{4}$$

If muons are present in matter, the following purely leptonic reactions are operative

$$\mu^- \rightleftarrows e^- + \bar{\nu}_e + \nu_\mu \quad (\text{muon decay}), \tag{5}$$

$$\mu^- + \nu_e \rightleftarrows e^- + \nu_\mu \quad (\text{neutrino scattering}), \tag{6}$$

$$\mu^- + \bar{\nu}_\mu \rightleftarrows e^- + \bar{\nu}_e \quad (\text{antineutrino scattering}). \tag{7}$$

Stellar matter is in approximate β-equilibrium which implies $\mu_n + \mu_{\nu_l} = \mu_p + \mu_l$, where $l = \{e, \mu\}$. We assume that neutrino flavor conversion can be neglected, so there are four exactly conserved quantities: baryon number

$n_B = n_n + n_p$, electric charge (the system remains charge neutral $n_p = n_e + n_\mu$), and lepton numbers $n_{L_l} = n_l + n_{\nu_l} = Y_{L_l} n_B$ for each flavor l separately. Here Y_{L_l} are the lepton fractions, which have typical values $Y_{Le} = Y_{L\mu} = 0.1$ in the BNS mergers [18] and $Y_{Le} = Y_{L\mu} = 0.4$ in proto-neutron stars and supernovas [40–42]. Since there are 4 conserved quantities and 6 particle species, this leaves two chemical potentials (33) and (34) discussed below that are driven to zero by weak interactions on timescales that are potentially comparable to the density variations in a merger. In this paper, we calculate the resultant bulk viscosity.

A. Urca process rates

The neutron decay processes (1) and (3) can be written compactly as $n \to p + l^- + \bar{\nu}_l$, where l^- is an electron or muon and $\bar{\nu}_l$ is the corresponding antineutrino. Then, the rate of each of these processes can be written as

$$\Gamma_{n\to pl\bar{\nu}} = \int \frac{d^3p}{(2\pi)^3 2p_0} \int \frac{d^3p'}{(2\pi)^3 2p_0'} \int \frac{d^3k}{(2\pi)^3 2k_0} \int \frac{d^3k'}{(2\pi)^3 2k_0'} \sum |\mathcal{M}_{\rm Urca}|^2 \times \bar{f}(k)\bar{f}(p)\bar{f}(k')f(p')(2\pi)^4\delta^{(4)}(k + p + k' - p'), \tag{8}$$

where $f(p)$ is the Fermi distribution function, $\bar{f}(p) \equiv 1 - f(p)$, and the mapping between the particles and their momenta is as follows: $(l) \to k$, $(\nu_l/\bar{\nu}_l) \to k'$, $(p) \to p$, and $(n) \to p'$. Similarly, the lepton capture processes (2) and (4) can be written as $p + l^- \to n + \nu_l$ and the corresponding rate is given by

$$\Gamma_{pl\to n\nu} = \int \frac{d^3p}{(2\pi)^3 2p_0} \int \frac{d^3p'}{(2\pi)^3 2p_0'} \int \frac{d^3k}{(2\pi)^3 2k_0} \int \frac{d^3k'}{(2\pi)^3 2k_0'} \sum |\mathcal{M}_{\rm Urca}|^2 \times f(k)f(p)\bar{f}(k')\bar{f}(p')(2\pi)^4\delta(k + p - k' - p'). \tag{9}$$

The matrix element of these processes is [45]

$$\sum |\mathcal{M}_{\rm Urca}|^2 = 32 G_F^2 \cos^2\theta_c [(1 + g_A)^2 (k \cdot p)(k' \cdot p') + (1 - g_A)^2 (k \cdot p')(k' \cdot p) + (g_A^2 - 1) m_n^* m_p^* (k \cdot k')], \tag{10}$$

where $G_F = 1.166 \times 10^{-5}$ GeV^{-2} is the Fermi coupling constant, θ_c is the Cabibbo angle ($\cos\theta_c = 0.974$), $g_A = 1.26$ is the axial-vector coupling constant, and m_n^* and m_p^* are the effective masses of neutron and proton, respectively. Because $g_A \approx 1$, the second and the third terms in Eq. (10) are suppressed as compared to the first one so we neglect them in our further computations.

The equilibration rates given by Eq. (8) and (9) can be computed once we specify the spectrum of strongly interacting nucleons. We apply the covariant density functional theory (CDF) of nuclear matter which is based on phenomenological baryon-meson Lagrangians introduced ba Walecka, Boguta-Bodmer and others [46,47].

The Lagrangian density of matter is given by

$$\mathcal{L} = \sum_N \bar{\psi}_N \left[\gamma^\mu \left(i\partial_\mu - g_\omega \omega_\mu - \frac{1}{2} g_\rho \boldsymbol{\tau} \cdot \boldsymbol{\rho}_\mu \right) - m_N^* \right] \psi_N + \sum_\lambda \bar{\psi}_\lambda (i\gamma^\mu \partial_\mu - m_\lambda)\psi_\lambda, + \frac{1}{2}\partial^\mu\sigma\partial_\mu\sigma - \frac{1}{2} m_\sigma^2 \sigma^2 - U(\sigma) - \frac{1}{4}\omega^{\mu\nu}\omega_{\mu\nu} + \frac{1}{2} m_\omega^2 \omega^\mu \omega_\mu - \frac{1}{4}\boldsymbol{\rho}^{\mu\nu} \cdot \boldsymbol{\rho}_{\mu\nu} + \frac{1}{2} m_\rho^2 \boldsymbol{\rho}^\mu \cdot \boldsymbol{\rho}_\mu, \tag{11}$$

where N sums over nucleons, ψ_N are the nucleonic Dirac fields with effective masses $m_N^* = m_N - g_\sigma \sigma$, with m_N being the nucleon mass in vacuum; σ, ω_μ, $\boldsymbol{\rho}_\mu$ are, respectively, the scalar-isoscalar, vector-isoscalar and vector-isovector meson fields which mediate the interaction between baryons; $\omega_{\mu\nu} = \partial_\mu\omega_\nu - \partial_\nu\omega_\mu$ and $\boldsymbol{\rho}_{\mu\nu} = \partial_\mu\boldsymbol{\rho}_\nu - \partial_\nu\boldsymbol{\rho}_\mu$ are the field strength tensors of vector mesons; m_i are the meson masses and g_i are the baryon-meson couplings with $i = \sigma,\ \omega,\ \rho$; finally, $U(\sigma)$ is the self-interaction potential of scalar meson field. The leptonic part of the Lagrangian is given by the second sum in Eq. (11), where ψ_λ, $\lambda \in (e^-, \mu^-, \nu_e, \nu_\mu)$, are the free Dirac fields of leptons with masses $m_{e^-} = 0.51$ MeV, $m_{\mu^-} = 105.7$ MeV, and $m_{\nu_e} = m_{\nu_\mu} = 0$. In the following we will adopt two different parametrizations of Lagrangian (11), specifically, the model DDME2 [38] in which the nucleon-meson couplings are density-dependent and $U(\sigma) = 0$, and the model NL3 [39], which has density-independent nucleon-meson couplings but nonzero self-interaction among σ-meson fields, which is contained in the potential $U(\sigma) = g_2\sigma^3/3 + g_3\sigma^4/4$.

The spectrum of nucleonic excitations derived from Eq. (11) in the mean-field approximation is given by [46]

$$E_k = \sqrt{k^2 + m_N^{*2}} + g_\omega \omega_0 + I_3 g_\rho \rho_{03} + \Sigma_r, \qquad (12)$$

where I_3 is the third component of the nucleon isospin, Σ_r is so-called rearrangement self-energy [48] which should be introduced to maintain the thermodynamical consistency (specifically the energy conservation and fulfillment of the Hugenholtz-van Hove theorem) of the system in the case of density-dependent couplings. Defining the nucleon effective chemical potentials as $\mu_N^* = \mu_N - g_\omega \omega_0 - I_3 g_\rho \rho_3^0 - \Sigma_r$ we can write the argument of nucleon Fermi-functions as $E_k - \mu_N = \sqrt{k^2 + m_N^{*2}} - \mu_N^*$ which formally coincides with the spectrum of free nucleons with effective masses and effective chemical potentials.

The details of computation of the phase-space integrals in Eqs. (8) and (9) are given in Appendix A. The final result reads

$$\begin{aligned}\Gamma_{n\to pl\bar{\nu}}(\mu_{\Delta_l}) = -\frac{G^2T^4}{(2\pi)^5}\int_{-\infty}^{\infty} dy \int_0^{\infty} dx[(\mu_{\nu_l} + \mu_n^* + yT)^2 - m_n^{*2} - x^2T^2] \\ \times [(\mu_l + \mu_p^* + \bar{y}_l T)^2 - m_l^2 - m_p^{*2} - x^2T^2] \\ \times \int_{m_l/T-\alpha_l}^{\alpha_p+\bar{y}_l} dz\, \bar{f}(z) f(z-\bar{y}_l)\theta_x \int_{\alpha_{\nu_l}}^{\infty} dz'\, f(z'+y)\bar{f}(z')\theta_y, \end{aligned} \qquad (13)$$

$$\begin{aligned}\Gamma_{pl\to n\nu}(\mu_{\Delta_l}) = \frac{G^2T^4}{(2\pi)^5}\int_{-\infty}^{\infty} dy \int_0^{\infty} dx[(\mu_{\nu_l} + \mu_n^* + yT)^2 - m_n^{*2} - x^2T^2] \\ \times [(\mu_l + \mu_p^* + \bar{y}_l T)^2 - m_l^2 - m_p^{*2} - x^2T^2] \\ \times \int_{m_l/T-\alpha_l}^{\alpha_p+\bar{y}_l} dz\, f(z) f(\bar{y}_l - z)\theta_x \int_{-\alpha_{\nu_l}}^{\alpha_n+y} dz'\, f(z'-y)\bar{f}(z')\theta_z, \end{aligned} \qquad (14)$$

where $G = G_F \cos\theta_c (1 + g_A)$, $\alpha_j = \mu_j^*/T$ for baryons and $\alpha_j = \mu_j/T$ for leptons, $\bar{y}_l = y + \mu_{\Delta_l}/T$ with $\mu_{\Delta_l} = \mu_n + \mu_{\nu_l} - \mu_p - \mu_l$ being the chemical potential imbalances (see Sec. III). The θ-functions in Eqs. (13) and (14) impose the constraints

$$\theta_x:\ (z_k - x)^2 \le (z - \alpha_p - \bar{y}_l)^2 - m_p^{*2}/T^2 \le (z_k + x)^2, \qquad (15)$$

$$\theta_y:\ (z_k' - x)^2 \le (z' + \alpha_n + y)^2 - m_n^{*2}/T^2 \le (z_k' + x)^2, \qquad (16)$$

$$\theta_z:\ (z_k' - x)^2 \le (z' - \alpha_n - y)^2 - m_n^{*2}/T^2 \le (z_k' + x)^2. \qquad (17)$$

The integration variables y and x are the transferred energy and momentum, respectively, normalized by the temperature; the variables z and z' are the normalized-by-temperature lepton and neutrino energies, respectively, computed from their chemical potentials, and $z_k = \sqrt{(z+\alpha_l)^2 - m_l^2/T^2}$ and $z_k' = z' \mp \alpha_{\nu_l}$ are the normalized-by-temperature momenta of the lepton and the antineutrino/neutrino, respectively. The rates of the inverse processes can be obtained from Eqs. (13) and (14) by interchanging $f(p_i) \leftrightarrow \bar{f}(p_i)$ for all particles.

In beta equilibrium we have $\mu_{\Delta_l} = 0$ and the rates of the direct and inverse processes are equal for each lepton flavor: $\Gamma_{n\to pl\bar{\nu}} = \Gamma_{pl\bar{\nu}\to n} \equiv \Gamma_{n\leftrightarrow pl\bar{\nu}}$, $\Gamma_{pl\to n\nu} = \Gamma_{n\nu\to pl} \equiv \Gamma_{pl\leftrightarrow n\nu}$. For small departures from β-equilibrium $\mu_{\Delta_l} \ll T$, we can assume linear response where the net proton production rate due to the neutron decay and its inverse processes is $\Gamma_{n\to pl\bar{\nu}} - \Gamma_{pl\bar{\nu}\to n} = \lambda_{n\leftrightarrow pl\bar{\nu}}\mu_{\Delta_l}$. Similarly, the net proton production rate due to the inverse and direct lepton capture processes is $\Gamma_{n\nu\to pl} - \Gamma_{pl\to n\nu} = \lambda_{pl\leftrightarrow n\nu}\mu_{\Delta_l}$. Pushing the system out of beta equilibrium by a chemical potential μ_{Δ_l} just replaces one power of T in the rate with a power of μ_{Δ_l}, so the expansion coefficients $\lambda_{n\leftrightarrow pl\bar{\nu}}$ and $\lambda_{pl\leftrightarrow n\nu}$ (see Appendix A) are given by

$$\lambda_{n\leftrightarrow pl\bar{\nu}} = \left(\frac{\partial\Gamma_{n\to pl\bar{\nu}}}{\partial\mu_{\Delta_l}} - \frac{\partial\Gamma_{pl\bar{\nu}\to n}}{\partial\mu_{\Delta_l}}\right)\Bigg|_{\mu_{\Delta_l}=0} = \frac{\Gamma_{n\leftrightarrow pl\bar{\nu}}}{T}, \qquad (18)$$

$$\lambda_{pl\leftrightarrow n\nu} = \left(\frac{\partial\Gamma_{n\nu\to pl}}{\partial\mu_{\Delta_l}} - \frac{\partial\Gamma_{pl\to n\nu}}{\partial\mu_{\Delta_l}}\right)\Bigg|_{\mu_{\Delta_l}=0} = \frac{\Gamma_{pl\leftrightarrow n\nu}}{T}. \qquad (19)$$

B. Lepton process rates

The general form of the lepton reaction rates (5), (6) and (7) reads

$$\Gamma_{\mu\to e\bar{\nu}\nu} = \int d\Omega_k \sum |\mathcal{M}_{\rm lep}|^2 f(k_\mu)\bar{f}(k_e)\bar{f}(k_{\bar{\nu}_e})\bar{f}(k_{\nu_\mu})(2\pi)^4\delta^{(4)}(k_e + k_{\bar{\nu}_e} + k_{\nu_\mu} - k_\mu), \tag{20}$$

$$\Gamma_{\mu\nu\to e\nu} = \int d\Omega_k \sum |\mathcal{M}_{\rm lep}|^2 f(k_\mu)f(k_{\nu_e})\bar{f}(k_e)\bar{f}(k_{\nu_\mu})(2\pi)^4\delta^{(4)}(k_e + k_{\nu_\mu} - k_{\nu_e} - k_\mu), \tag{21}$$

$$\Gamma_{\mu\bar{\nu}\to e\bar{\nu}} = \int d\Omega_k \sum |\mathcal{M}_{\rm lep}|^2 f(k_\mu)f(k_{\bar{\nu}_\mu})\bar{f}(k_e)\bar{f}(k_{\bar{\nu}_e})(2\pi)^4\delta^{(4)}(k_e + k_{\bar{\nu}_e} - k_{\bar{\nu}_\mu} - k_\mu), \tag{22}$$

where the short-hand notation $d\Omega_k$ is the Lorentz-invariant momentum phase-space element, i.e.,

$$\int d\Omega_k = \int \frac{d^3k_e}{(2\pi)^3 2k_{0e}} \int \frac{d^3k_\mu}{(2\pi)^3 2k_{0\mu}} \int \frac{d^3k_{\nu_e/\bar{\nu}_e}}{(2\pi)^3 2k_{0\nu_e/\bar{\nu}_e}} \int \frac{d^3k_{\nu_\mu/\bar{\nu}_\mu}}{(2\pi)^3 2k_{0\nu_\mu/\bar{\nu}_\mu}}. \tag{23}$$

The spin-averaged relativistic matrix element of lepton reactions reads [43]

$$\sum |\mathcal{M}_{\rm lep}|^2 = 128 G_F^2 (k_e \cdot k_{\nu_\mu/\bar{\nu}_\mu})(k_{\nu_e/\bar{\nu}_e} \cdot k_\mu). \tag{24}$$

Computation of lepton process rates can be performed analogously to the Urca process rates. The final expressions suitable for numerical evaluation are

$$\begin{aligned}\Gamma_{\mu\to e\bar{\nu}\nu}(\mu_\Delta^L) = &-\frac{4G_F^2T^4}{(2\pi)^5}\int_{-\infty}^{\infty} dy \int_0^\infty dx[(\mu_e + \mu_{\nu_\mu} + \tilde{y}T)^2 - m_e^2 - x^2T^2] \\ &\times [(\mu_{\nu_e} + \mu_\mu + yT)^2 - m_\mu^2 - x^2T^2] \\ &\times \int_{m_e/T-\alpha_e}^{\alpha_{\nu_\mu}+\tilde{y}} dz\, \bar{f}(z) f(z-\tilde{y})\theta_x^L \int_{\alpha_{\nu_e}}^\infty dz'\, f(z'+y)\bar{f}(z')\theta_y^L,\end{aligned} \tag{25}$$

$$\begin{aligned}\Gamma_{\mu\nu\to e\nu}(\mu_\Delta^L) = &\frac{4G_F^2T^4}{(2\pi)^5}\int_{-\infty}^{\infty} dy \int_0^\infty dx[(\mu_e + \mu_{\nu_\mu} + \tilde{y}T)^2 - m_e^2 - x^2T^2] \\ &\times [(\mu_{\nu_e} + \mu_\mu + yT)^2 - m_\mu^2 - x^2T^2] \\ &\times \int_{m_e/T-\alpha_e}^{\alpha_{\nu_\mu}+\tilde{y}} dz\, \bar{f}(z) \bar{f}(\tilde{y}-z)\theta_x^L \int_{-\alpha_{\nu_e}}^{\alpha_\mu+y} dz'\, \bar{f}(z'-y) f(z')\theta_z^L,\end{aligned} \tag{26}$$

$$\begin{aligned}\Gamma_{\mu\bar{\nu}\to e\bar{\nu}}(\mu_\Delta^L) = &\frac{4G_F^2T^4}{(2\pi)^5}\int_{-\infty}^{\infty} dy \int_0^\infty dx[(\mu_e + \mu_{\nu_\mu} + \tilde{y}T)^2 - m_e^2 - x^2T^2] \\ &\times [(\mu_{\nu_e} + \mu_\mu + yT)^2 - m_\mu^2 - x^2T^2] \\ &\times \int_{z_{\rm min}}^\infty dz\, \bar{f}(z) f(z-\tilde{y})\theta_x^L \int_{\alpha_{\nu_e}}^\infty dz'\, f(z'+y)\bar{f}(z')\theta_y^L,\end{aligned} \tag{27}$$

where $\mu_\Delta^L \equiv \mu_\mu + \mu_{\nu_e} - \mu_e - \mu_{\nu_\mu} = \mu_{\Delta_e} - \mu_{\Delta_\mu}$ is the chemical imbalance for leptons, $\tilde{y} = y + \mu_\Delta^L/T$, $z_{\rm min} = \max\{m_e/T - \alpha_e; \alpha_{\nu_\mu} + \tilde{y}\}$, and the θ-functions impose the constraints

$$\theta_x^L:\ (z_k - x)^2 \le (z - \alpha_{\nu_\mu} - \tilde{y})^2 \le (z_k + x)^2, \tag{28}$$

$$\theta_y^L:\ (z_k' - x)^2 \le (z' + \alpha_\mu + y)^2 - m_\mu^2/T^2 \le (z_k' + x)^2, \tag{29}$$

$$\theta_z^L:\ (z_k' - x)^2 \le (z' - \alpha_\mu - y)^2 - m_\mu^2/T^2 \le (z_k' + x)^2, \tag{30}$$

with $z_k = \sqrt{(z+\alpha_e)^2 - m_e^2/T^2}$ and $z_k' = z' \mp \alpha_{\nu_e}$ for θ_y/θ_z.

III. BULK VISCOSITY OF *npeμ* MATTER

In this section, we derive a microscopic formula for the bulk viscosity of neutrino-trapped $npe\mu$ matter arising from the Urca processes (1)–(4). In the temperature and density range where the neutrinos are trapped the β-equilibration rates are much higher than the characteristic frequency of density oscillations; this corresponds to the *fast equilibration regime* [21]. Then the analysis can be restricted to the "subthermal" case, where the matter is only slightly perturbed from equilibrium.

Consider now small-amplitude density oscillations in nuclear matter with a given frequency ω for which we can write $n_B(t) = n_{B0} + \delta n_B(t)$ and $n_{L_l}(t) = n_{L_l 0} + \delta n_{L_l}(t)$, where $\delta n_B(t)$, $\delta n_{L_l}(t) \sim e^{i\omega t}$. The baryon and lepton conservation laws in the comoving frame imply

$$\delta n_B = -n_{B0}\frac{\theta}{i\omega}, \quad \delta n_{L_l} = -n_{L_l 0}\frac{\theta}{i\omega}, \quad l = \{e, \mu\}, \tag{31}$$

where $\theta = \partial_i v^i$ is the fluid velocity divergence.

The perturbations of particle densities can be separated into local equilibrium and nonequilibrium parts

$$n_j(t) = n_{j0} + \delta n_j(t), \quad \delta n_j(t) = \delta n_j^{\mathrm{eq}}(t) + \delta n_j'(t), \tag{32}$$

where $j = \{n, p, e, \mu, \nu_e, \nu_\mu\}$ labels the particles. The variations $\delta n_j^{\mathrm{eq}}(t)$ denote the shift of the equilibrium state for the instantaneous values of the baryon and lepton densities $n_B(t)$ and $n_{L_l}(t)$, whereas $\delta n_j'(t)$ denote the deviations of the corresponding densities from their equilibrium values.

The compression and rarefaction drives the system out of chemical equilibrium leading to nonzero $\delta n_j'(t)$, and, subsequently, to chemical imbalances $\mu_{\Delta_l} = \delta\mu_n + \delta\mu_{\nu_l} - \delta\mu_p - \delta\mu_l$, which can be written as

$$\mu_{\Delta_e} = A_n\delta n_n + A_{\nu_e}\delta n_{\nu_e} - A_p\delta n_p - A_e\delta n_e, \tag{33}$$

$$\mu_{\Delta_\mu} = A_n\delta n_n + A_{\nu_\mu}\delta n_{\nu_\mu} - A_p\delta n_p - A_\mu\delta n_\mu, \tag{34}$$

where $A_n = A_{nn} - A_{pn}$, $A_p = A_{pp} - A_{np}$, and $A_l = A_{ll}$, $A_{\nu_l} = A_{\nu_l\nu_l}$ with

$$A_{ij} = \left(\frac{\partial\mu_i}{\partial n_j}\right)_0, \tag{35}$$

and index 0 refers to the equilibrium state. The nuclear off-diagonal elements A_{np} and A_{pn} are nonzero because of the cross-species strong interaction between neutrons and protons. The computation of susceptibilities A_{ij} is performed in Appendix B.

To proceed further we need to determine how the lepton reactions (5)–(7) affect the bulk viscosity from the Urca processes (1)–(4). Typically, we deal with two limiting cases: (a) fast lepton-equilibration limit, i.e., the lepton process rates are much higher than Urca process rates; (b) slow lepton-equilibration limit, where the lepton process rates are much lower than Urca process rates. We derive analytic expressions for the bulk viscosity in terms of equilibration rates and particle susceptibilities in these two limiting cases in the next two subsections.

A. Fast lepton-equilibration limit

In this case, the chemical equilibration among leptons (processes (5), (6), (7)) takes place much faster than the equilibration between baryons and leptons, therefore the condition $\mu_e - \mu_{\nu_e} = \mu_\mu - \mu_{\nu_\mu}$ can be assumed to be satisfied while studying the bulk viscosity from the Urca processes. This implies $\mu_{\Delta_e} = \mu_{\Delta_\mu} \equiv \mu_\Delta$, i.e., the electronic and muonic Urca processes are described by a single chemical potential shift from equilibrium. The rate equations which take into account the loss and gain of particles read

$$\frac{\partial}{\partial t}\delta n_n(t) = -\theta n_{n0} - (\lambda_e + \lambda_\mu)\mu_\Delta(t), \tag{36}$$

$$\frac{\partial}{\partial t}\delta n_p(t) = -\theta n_{p0} + (\lambda_e + \lambda_\mu)\mu_\Delta(t), \tag{37}$$

$$\frac{\partial}{\partial t}\delta n_e(t) = -\theta n_{e0} + \lambda_e\mu_\Delta(t) + I_L, \tag{38}$$

$$\frac{\partial}{\partial t}\delta n_\mu(t) = -\theta n_{\mu 0} + \lambda_\mu\mu_\Delta(t) - I_L, \tag{39}$$

where $\lambda_e = \lambda_{n\leftrightarrow pe\bar{\nu}} + \lambda_{pe\leftrightarrow n\nu}$ and $\lambda_\mu = \lambda_{n\leftrightarrow p\mu\bar{\nu}} + \lambda_{p\mu\leftrightarrow n\nu}$ are the summed equilibration rates of the electron and muon Urca reactions, respectively. The quantity I_L is the summed rate of the lepton reactions (5), (6), (7), which arises as a result of an almost vanishing shift $\mu_{\Delta_e} - \mu_{\Delta_\mu} \ll \mu_\Delta$ but cannot be neglected because the relevant λ-coefficient can be very large, as already discussed in Ref. [49].

Only two of the balance equations are independent (one for a baryon and one for a lepton) as the others can be obtained from them via exploiting the conditions of charge neutrality $\delta n_p = \delta n_e + \delta n_\mu$ and baryon conservation $\delta n_B = \delta n_n + \delta n_p$. The balance equations for neutrinos are obtained from Eqs. (38) and (39) and the constraints $\delta n_{L_l} = \delta n_l + \delta n_{\nu_l}$.

The equilibrium with respect to lepton reactions implies

$$\begin{aligned}&\delta\mu_\mu + \delta\mu_{\nu_e} - \delta\mu_e - \delta\mu_{\nu_\mu}\\ &\quad = A_\mu\delta n_\mu + A_{\nu_e}\delta n_{\nu_e} - A_e\delta n_e - A_{\nu_\mu}\delta n_{\nu_\mu} = 0,\end{aligned} \tag{40}$$

which gives the constraints

$$\delta n_e = \frac{(A_\mu + A_{\nu_\mu})\delta n_p + A_{\nu_e}\delta n_{L_e} - A_{\nu_\mu}\delta n_{L_\mu}}{A_L}, \quad (41)$$

$$\delta n_\mu = \frac{(A_e + A_{\nu_e})\delta n_p - A_{\nu_e}\delta n_{L_e} + A_{\nu_\mu}\delta n_{L_\mu}}{A_L}, \quad (42)$$

with $A_L = A_e + A_{\nu_e} + A_\mu + A_{\nu_\mu}$. Substituting these expressions into Eq. (33) we find

$$\mu_\Delta = A_L^{-1}[(N_n - N_p)\delta n_n + N_p\delta n_B + N_e\delta n_{L_e} + N_\mu\delta n_{L_\mu}], \quad (43)$$

where

$$N_n = A_L A_n, \quad (44)$$

$$N_p = -A_p A_L - (A_e + A_{\nu_e})(A_\mu + A_{\nu_\mu}), \quad (45)$$

$$N_B = N_n - N_p = A_L(A_n + A_p) + (A_e + A_{\nu_e})(A_\mu + A_{\nu_\mu}), \quad (46)$$

$$N_e = A_{\nu_e}(A_\mu + A_{\nu_\mu}), \quad (47)$$

$$N_\mu = A_{\nu_\mu}(A_e + A_{\nu_e}). \quad (48)$$

Next we substitute μ_Δ in Eq. (36), assume that the time-dependence of density perturbations is given by $\delta n_j(t) \sim e^{i\omega t}$ and take into account Eq. (31) to obtain

$$\begin{aligned} &i\omega\delta n_n + \theta n_{n0} + \lambda A_L^{-1}[N_B\delta n_n + N_p\delta n_B + N_e\delta n_{L_e} + N_\mu\delta n_{L_\mu}] \\ &= A_L^{-1}[(i\omega A_L + \lambda N_B)\delta n_n + \lambda N_p\delta n_B + \theta n_{n0}A_L + \lambda(N_e\delta n_{L_e} + N_\mu\delta n_{L_\mu})] = 0, \end{aligned} \quad (49)$$

with $\lambda = \lambda_e + \lambda_\mu$. Solving for δn_n gives

$$\delta n_n = \frac{\theta}{i\omega}\frac{\lambda N_p n_{B0} + \lambda(N_e n_{L_e 0} + N_\mu n_{L_\mu 0}) - i\omega n_{n0}A_L}{i\omega A_L + \lambda N_B}. \quad (50)$$

Under similar assumptions Eq. (41) gives

$$\begin{aligned} \delta n_e = -\frac{\theta}{i\omega}\frac{1}{(i\omega A_L + \lambda N_B)}\{&i\omega(A_\mu + A_{\nu_\mu})n_{p0} + \lambda A_n(A_\mu + A_{\nu_\mu})n_{B0} \\ &+ (i\omega + \lambda A_2)A_{\nu_e}n_{L_e 0} - [i\omega + \lambda(A_n + A_p)]A_{\nu_\mu}n_{L_\mu 0}\}, \end{aligned} \quad (51)$$

where we exploited the relations

$$N_B A_{\nu_e} + N_e(A_\mu + A_{\nu_\mu}) = A_{\nu_e}A_L A_2, \quad (52)$$

$$N_B A_{\nu_\mu} - N_\mu(A_\mu + A_{\nu_\mu}) = A_{\nu_\mu}A_L(A_n + A_p), \quad (53)$$

and

$$A_1 \equiv A_n + A_p + A_e + A_{\nu_e}, \quad (54)$$

$$A_2 \equiv A_n + A_p + A_\mu + A_{\nu_\mu}. \quad (55)$$

The equilibrium shifts of neutron and electron densities can be found from the $\lambda \to \infty$ limit of Eqs. (50) and (51), respectively (see also Ref. [24])

$$\delta n_n^{\rm eq} = \frac{\theta}{i\omega N_B}\{[-A_p A_L - (A_e + A_{\nu_e})(A_\mu + A_{\nu_\mu})]n_{B0} + A_{\nu_e}(A_\mu + A_{\nu_\mu})n_{L_e 0} + A_{\nu_\mu}(A_e + A_{\nu_e})n_{L_\mu 0}\}, \quad (56)$$

$$\delta n_e^{\rm eq} = -\frac{\theta}{i\omega N_B}[A_n(A_\mu + A_{\nu_\mu})n_{B0} + A_{\nu_e}A_2 n_{L_e 0} - A_{\nu_\mu}(A_n + A_p)n_{L_\mu 0}]. \quad (57)$$

Finally, for the nonequilibrium shifts, we find

$$\delta n_n' = -\theta A_L \frac{N_B n_{n0} + N_p n_{B0} + N_e n_{L_e 0} + N_\mu n_{L_\mu 0}}{N_B(i\omega A_L + \lambda N_B)}, \tag{58}$$

$$\delta n_e' = \frac{\theta(A_\mu + A_{\nu_\mu})}{N_B(i\omega A_L + \lambda N_B)}(N_n n_{n0} + N_p n_{p0} + N_e n_{L_e 0} + N_\mu n_{L_\mu 0}), \tag{59}$$

which can be written in a compact form

$$\delta n_n' = -\frac{\theta C}{B(i\omega + \lambda B)}, \tag{60}$$

$$\delta n_e' = \frac{A_\mu + A_{\nu_\mu}}{A_L}\frac{\theta C}{B(i\omega + \lambda B)}, \tag{61}$$

where $B = N_B/A_L$, and $C = (N_n n_{n0} + N_p n_{p0} + N_e n_{L_e 0} + N_\mu n_{L_\mu 0})/A_L$.

The full expression for the out-of-equilibrium pressure is given by

$$\begin{aligned} p(t) &= p(n_j(t)) = p[n_{j0} + \delta n_j^{\mathrm{eq}}(t)] + \delta p'(t) \\ &= p^{\mathrm{eq}}(t) + \delta p'(t), \end{aligned} \tag{62}$$

where the nonequilibrium part of the pressure, referred to as bulk viscous pressure, is given by

$$\Pi \equiv \delta p' = \sum_j \left(\frac{\partial p}{\partial n_j}\right)_0 \delta n_j'. \tag{63}$$

Using the Gibbs-Duhem relation $dp = sdT + \sum_i n_i d\mu_i$, which is valid also out of equilibrium, we can write [50]

$$c_j \equiv \left(\frac{\partial p}{\partial n_j}\right)_0 = \sum_i n_{i0}\left(\frac{\partial \mu_i}{\partial n_j}\right)_0 = \sum_i n_{i0} A_{ij}. \tag{64}$$

Then, using also the relations $\delta n_p' = -\delta n_n'$, $\delta n_\mu' = \delta n_p' - \delta n_e'$, $\delta n_{\nu_l}' = -\delta n_l'$, we obtain

$$\begin{aligned} \Pi = \frac{\theta C}{A_L B(i\omega + \lambda B)}[&-(c_n - c_p - c_\mu + c_{\nu_\mu})A_L \\ &+ (c_e - c_{\nu_e} - c_\mu + c_{\nu_\mu})(A_\mu + A_{\nu_\mu})]. \end{aligned} \tag{65}$$

Writing out Eq. (64) for each particle species and recalling the definitions of relations $A_{pn} = A_{np} = A_{nn} - A_n = A_{pp} - A_p$ we find

$$c_l = n_{l0} A_l, \qquad c_{\nu_l} = n_{\nu_l 0} A_{\nu_l}, \tag{66}$$

$$c_n = n_{n0} A_{nn} + n_{p0} A_{pn} = n_{B0} A_{nn} - n_{p0} A_n, \tag{67}$$

$$c_p = n_{p0} A_{pp} + n_{n0} A_{np} = n_{B0}(A_{nn} - A_n) + n_{p0} A_p, \tag{68}$$

which allows us to write (65) as

$$\Pi = -\frac{\theta C^2}{B(i\omega + \lambda B)}. \tag{69}$$

The bulk viscosity is defined as the real part of $-\Pi/\theta$, i.e.,

$$\zeta = \frac{C^2}{B}\frac{\gamma}{\omega^2 + \gamma^2}, \qquad \gamma = \lambda B. \tag{70}$$

Bulk viscosity given by Eq. (70) has the classic resonant form which depends on two quantities: the thermodynamic prefactor C^2/B which depends only on the EoS, and the relaxation rate γ which depends on the weak interaction rates of electron and muon Urca processes. The limit of the absence of muons is obtained from the above equations by setting $n_\mu = n_{\nu_\mu} = 0$ and taking the limit $A_\mu, A_{\nu_\mu} \to \infty$. Then $A_L = A_\mu + A_{\nu_\mu}$, and the previous expressions (45) and (47) reduce to

$$N_p = -(A_p + A_e + A_{\nu_e})A_L, \qquad N_e = A_{\nu_e} A_L, \tag{71}$$

and

$$B = A_1, \quad C = A_n n_{n0} - A_p n_{p0} - A_e n_{e0} + A_{\nu_e} n_{\nu_e 0}. \tag{72}$$

The coefficients B and C coincide with those given in our previous work [22].

B. Slow lepton-equilibration limit

When the lepton equilibration processes (5), (6), (7) are slow compared to the Urca processes, i.e., $\mu_{\Delta_e} \neq \mu_{\Delta_\mu}$, there are two independent shifts in this case. Now $I_L \simeq 0$, and rate equations take the form

$$\frac{\partial}{\partial t}\delta n_n(t) = -\theta n_{n0} - \lambda_e \mu_{\Delta_e}(t) - \lambda_\mu \mu_{\Delta_\mu}(t), \tag{73}$$

$$\frac{\partial}{\partial t}\delta n_p(t) = -\theta n_{p0} + \lambda_e \mu_{\Delta_e}(t) + \lambda_\mu \mu_{\Delta_\mu}(t), \tag{74}$$

$$\frac{\partial}{\partial t}\delta n_e(t) = -\theta n_{e0} + \lambda_e \mu_{\Delta_e}(t), \tag{75}$$

$$\frac{\partial}{\partial t}\delta n_\mu(t) = -\theta n_{\mu 0} + \lambda_\mu \mu_{\Delta_\mu}(t). \tag{76}$$

Substituting Eqs. (33) and (34) in the rate equations and assuming the same time-dependence of perturbation as above we find

$$i\omega\delta n_n = -n_{n0}\theta - (\lambda_e + \lambda_\mu)A_n\delta n_n + (\lambda_e + \lambda_\mu)A_p\delta n_p - \lambda_e A_{\nu_e}\delta n_{\nu_e} + \lambda_e A_e\delta n_e - \lambda_\mu A_{\nu_\mu}\delta n_{\nu_\mu} + \lambda_\mu A_\mu\delta n_\mu, \tag{77}$$

$$i\omega\delta n_e = -n_{e0}\theta + \lambda_e A_n\delta n_n - \lambda_e A_p\delta n_p + \lambda_e A_{\nu_e}\delta n_{\nu_e} - \lambda_e A_e\delta n_e. \tag{78}$$

This system of equations is closed upon using the relations $\delta n_p + \delta n_n = \delta n_B$, $\delta n_e + \delta n_\mu = \delta n_p$, $\delta n_{L_e} = \delta n_e + \delta n_{\nu_e}$, and $\delta n_{L_\mu} = \delta n_\mu + \delta n_{\nu_\mu}$, which leads us to ($\lambda \equiv \lambda_e + \lambda_\mu$)

$$\delta n_e = \frac{-n_{e0}\theta + \lambda_e(A_n + A_p)\delta n_n - \lambda_e A_p\delta n_B + \lambda_e A_{\nu_e}\delta n_{L_e}}{i\omega + \lambda_e(A_e + A_{\nu_e})}, \tag{79}$$

$$i\omega\delta n_n = -n_{n0}\theta - (\lambda A_n + \lambda A_p + \lambda_\mu A_\mu + \lambda_\mu A_{\nu_\mu})\delta n_n + (\lambda_e A_e + \lambda_e A_{\nu_e} - \lambda_\mu A_\mu - \lambda_\mu A_{\nu_\mu})\delta n_e \tag{80}$$

$$+(\lambda A_p + \lambda_\mu A_\mu + \lambda_\mu A_{\nu_\mu})\delta n_B - \lambda_e A_{\nu_e}\delta n_{L_e} - \lambda_\mu A_{\nu_\mu}\delta n_{L_\mu}. \tag{81}$$

The coupled Eqs. (79) and (80) can be solved to find

$$\begin{aligned} D\delta n_n = -\frac{\theta}{i\omega}\{&i\omega[n_{n0}(i\omega + \lambda_e A_e + \lambda_e A_{\nu_e}) + n_{e0}(\lambda_e A_e + \lambda_e A_{\nu_e} - \lambda_\mu A_\mu - \lambda_\mu A_{\nu_\mu})] \\ &+ [i\omega(\lambda A_p + \lambda_\mu A_\mu + \lambda_\mu A_{\nu_\mu}) + \lambda_e\lambda_\mu((A_1 - A_n)(A_2 - A_n) - A_p^2)]n_{B0} \\ &- \lambda_e A_{\nu_e}[i\omega + \lambda_\mu(A_\mu + A_{\nu_\mu})]n_{L_e 0} - \lambda_\mu A_{\nu_\mu}[i\omega + \lambda_e(A_e + A_{\nu_e})]n_{L_\mu 0}\}, \end{aligned} \tag{82}$$

$$\begin{aligned} D\delta n_e = -\frac{\theta}{i\omega}\{&i\omega n_{e0}[i\omega + \lambda_\mu A_2 + \lambda_e(A_n + A_p)] - \lambda_e n_{B0}[A_p(i\omega + \lambda_\mu A_2) - \lambda_\mu(A_n + A_p)(A_2 - A_n)] \\ &+ \lambda_e n_{L_e 0}A_{\nu_e}(i\omega + \lambda_\mu A_2) + \lambda_e(A_n + A_p)i\omega n_{n0} - \lambda_e\lambda_\mu(A_n + A_p)A_{\nu_\mu}n_{L_\mu 0}\}, \end{aligned} \tag{83}$$

where

$$D = (i\omega + \lambda_e A_1)(i\omega + \lambda_\mu A_2) - \lambda_e\lambda_\mu(A_n + A_p)^2. \tag{84}$$

The equilibrium shifts $\delta n_f^{\rm eq}$ are found as the limit $\lambda_i \to \infty$ of Eqs. (82) and (83). However, as we showed in Ref. [24], one can use the quasiequilibrium solutions $\delta n_f^0 = -\theta n_{f0}/i\omega$ instead, which arise in the $\lambda_{e,\mu} \to 0$ limit of Eqs. (82) and (83). We then find

$$\delta n_n' = \frac{\theta}{i\omega}\frac{i\omega(\lambda_e C_1 + \lambda_\mu C_2) + \lambda_e\lambda_\mu[C_2(A_e + A_{\nu_e}) + C_1(A_\mu + A_{\nu_\mu})]}{(i\omega + \lambda_e A_1)(i\omega + \lambda_\mu A_2) - \lambda_e\lambda_\mu(A_n + A_p)^2}, \tag{85}$$

$$\delta n_e' = -\frac{\theta}{i\omega}\frac{i\omega\lambda_e C_1 + \lambda_e\lambda_\mu[A_2 C_1 - (A_n + A_p)C_2]}{(i\omega + \lambda_e A_1)(i\omega + \lambda_\mu A_2) - \lambda_e\lambda_\mu(A_n + A_p)^2}. \tag{86}$$

The bulk viscous pressure then reads

$$\Pi = \frac{\theta}{i\omega}\frac{i\omega(\lambda_e C_1^2 + \lambda_\mu C_2^2) + \lambda_e\lambda_\mu[A_1 C_2^2 + A_2 C_1^2 - 2(A_n + A_p)C_1 C_2]}{(i\omega + \lambda_e A_1)(i\omega + \lambda_\mu A_2) - \lambda_e\lambda_\mu(A_n + A_p)^2}, \tag{87}$$

where we used the relations

$$c_n - c_p - c_e + c_{\nu_e} = n_{n0}A_n - n_{p0}A_p - n_{e0}A_e + n_{\nu_e 0}A_{\nu_e} \equiv C_1, \tag{88}$$

$$c_n - c_p - c_\mu + c_{\nu_\mu} = n_{n0}A_n - n_{p0}A_p - n_{\mu 0}A_\mu + n_{\nu_\mu 0}A_{\nu_\mu} \equiv C_2. \tag{89}$$

Extracting the real part of Eq. (87) leads to the final expression of the bulk-viscosity

$$\zeta = \frac{\lambda_e\lambda_\mu\{\lambda_e[(A_n + A_p)C_1 - A_1 C_2]^2 + \lambda_\mu[(A_n + A_p)C_2 - A_2 C_1]^2\} + \omega^2(\lambda_e C_1^2 + \lambda_\mu C_2^2)}{\{\lambda_e\lambda_\mu[A_1 A_2 - (A_n + A_p)^2] - \omega^2\}^2 + \omega^2(\lambda_e A_1 + \lambda_\mu A_2)^2}. \tag{90}$$

If the muon contribution is neglected ($\lambda_\mu = 0$) Eq. (90) reduces to

$$\zeta_e = \frac{C_1^2}{A_1}\frac{\gamma_e}{\omega^2+\gamma_e^2}, \tag{91}$$

with $\gamma_e = \lambda_e A_1$, which coincides with the result of our previous work [22].

In the limit of high frequencies $\omega \gg \lambda A$ we find from Eq. (90)

$$\zeta = \frac{\lambda_e C_1^2 + \lambda_\mu C_2^2}{\omega^2} = \zeta_e + \zeta_\mu, \tag{92}$$

where ζ_e and ζ_μ are the contributions by electrons and muons, respectively.

In the low-frequency limit

$$\zeta = \frac{\lambda_e(C_1 - a_1 C_2)^2 + \lambda_\mu(C_2 - a_2 C_1)^2}{\lambda_e\lambda_\mu(A_n + A_p)^2(a_1 a_2 - 1)^2}, \tag{93}$$

with $a_1 = A_1/(A_n + A_p)$ and $a_2 = A_2/(A_n + A_p)$.

IV. NUMERICAL RESULTS

A. β-equilibration rates

We start the discussion by presenting the relevant thermodynamics of β-equilibrated, neutrino-trapped $npe\mu$ matter for two parametrizations of the density functional theory—the model DDME2 and the model NL3. The fractions of massive particles (i.e., nucleons, electrons and muons) are rather insensitive to the density and temperature. The particles abundances for $Y_{L_e} = Y_{L_\mu} = 0.1$ are as follows: neutron fraction—80%–82%, proton fraction—18%–20%, electron fraction—9.5%–10.5%, muon fraction—9%–10% for model DDME2; and neutron fraction—77%–81%, proton fraction—19%–23%, electron fraction—10%–12%, muon fraction—9%–11.5% for model NL3 in the range $5 \le T \le 50$ MeV and $1 \le n_B/n_0 \le 5$ with n_0 being the nuclear saturation density with the values $n_0 = 0.152$ fm^{-3} for model DDME2 and $n_0 = 0.153$ fm^{-3} for model NL3.

In contrast to the massive particles, the fractions of neutrinos are rather sensitive both to the density and temperature, see Fig. 1. At high temperatures and very low densities the net neutrino densities become negative in the DDME2 model, indicating that there are more antineutrinos than neutrinos in that regime. In the NL3 model instead only the low-temperature and the low-density regime is neutrino-dominated; the antineutrino population increases with the increase of both density and temperature. The reason for this behavior is the larger symmetry energy in the case of NL3 model which favors larger proton fractions as compared to the DDME2 model. Charge neutrality then requires larger electron and muon fractions and, therefore, smaller neutrino fractions for the given values of $Y_{L_l} = Y_l + Y_{\nu_l}$. Thus, we have an important difference in the composition of high-density and low-temperature, i.e., the degenerate regime of neutrino-trapped matter for these two models: while the trapped species are neutrinos in the DDEM2 matter, these are antineutrinos in the case of the NL3 model. This feature leads to qualitatively different behavior of β-equilibration rates and the bulk viscosity for these two models, see below.

1. Rates of Urca processes

Next, we turn to the discussion of the Urca process rates. As the neutron decay processes (1) and (3) involve

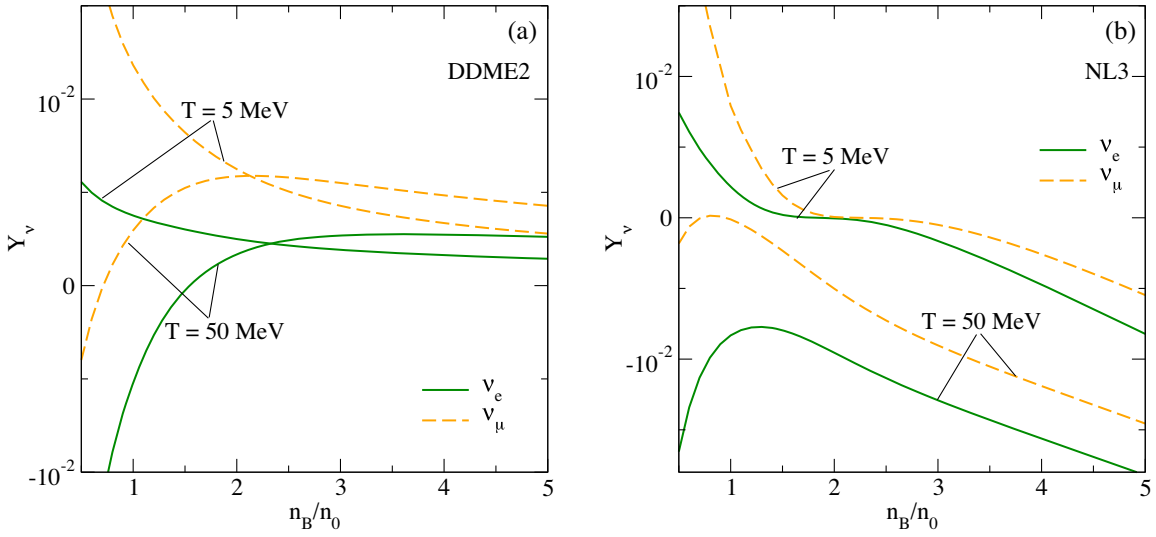

FIG. 1. Neutrino fractions in neutron-star-merger matter with $Y_{L_e} = Y_{L_\mu} = 0.1$ as functions of the baryon density n_B (in units of nuclear saturation density n_0) for two values of the temperatures for models DDME2 (a) and NL3 (b). At high temperatures and densities model NL3 becomes antineutrino-dominated.

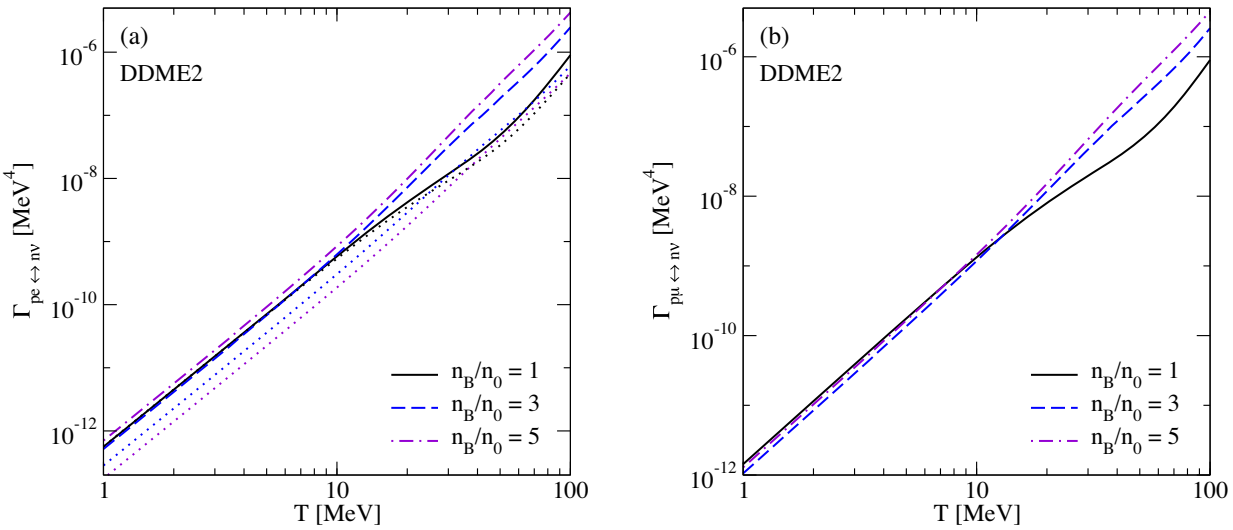

FIG. 2. The electron capture rate $\Gamma_{pe\leftrightarrow n\nu}$ (a) and the muon capture rate $\Gamma_{p\mu\leftrightarrow n\nu}$ (b) as functions of the temperature for various densities for the model DDME2. The neutron decay rates $\Gamma_{n\leftrightarrow pe\bar{\nu}}$ and $\Gamma_{n\leftrightarrow p\mu\bar{\nu}}$ are negligible compared to the lepton capture rates in the whole temperature-density range. The dotted lines in panel (a) show the electron capture rates computed in Ref. [22] within the approximation of nonrelativistic nucleons.

antineutrinos, their rates are expected to be much smaller than the lepton capture rates if the matter is neutrino-dominated, as discussed in Ref. [22]. Our numerical calculations show that the neutron decay rate is negligibly small if the neutrino chemical potential (for the given lepton species) satisfies the condition $\alpha_{\nu_l} = \mu_{\nu_l}/T \geq -3$. This condition is satisfied for DDME2 model in the whole temperature-density range of interest, therefore the dominant equilibration processes are the lepton capture processes. The rates of the electron and muon capture processes for model DDME2 are shown, respectively, in panels (a) and (b) of Fig. 2. At moderate temperatures, $T \leq 10$ MeV the lepton decay rates follow their low-temperature scaling given by Eq. (A31), i.e., increase cubically with the temperature. At higher temperatures, this scaling breaks down. However, the deviation of the exact equilibration rates from their low-temperature limit is within a few factors (see Appendix A). A comparison between the left and right panels in Fig. 2 shows that the electron and the muon capture rates are quite similar both qualitatively and quantitatively. In panel (a) we show also the electron capture rates which were computed in Ref. [22] in the approximation of nonrelativistic nucleons. As expected, the importance of relativistic corrections to the nucleon spectrum rises with the density, and at the density $n_B/n_0 = 5$ the full relativistic rate is around one order of magnitude larger than its nonrelativistic approximation.

Figure 3 shows the summed β-equilibration (Urca) rates $\Gamma_l = \Gamma_{n\leftrightarrow pl\bar{\nu}} + \Gamma_{pl\leftrightarrow n\nu}$ for the model NL3. In contrast to the model DDME2, the model NL3 features two different regimes of equilibration—the antineutrino-dominated regime in the low-temperature, high-density sector, where the dominant equilibration process is the neutron decay; and the neutrino-dominated regime in the high-temperature, low-density sector, where the dominant equilibration process is the lepton capture. As the antineutrino-dominated regime is realized at low temperatures and high densities where the matter is degenerate, the neutron decay rates follow the scaling $\propto T^3$ given by Eq. (A33). Numerically we find that the lepton capture rates are suppressed as long as the scaled-to-temperature neutrino chemical potential $\alpha_{\nu_l} \leq -6$. Although the net neutrino densities drop with the increase of temperature (see Fig. 1), their scaled chemical potentials increase (remaining negative) thus allowing the neutrinos to come into the game already at $\alpha_{\nu_l} \simeq -6$. At higher temperatures, the neutron decay rates become suppressed exponentially, and the lepton capture processes become dominant at $\alpha_{\nu_l} \simeq -3$. As a consequence, there is always a sharp minimum in the net equilibration rate which arises in the transition region between these two regimes. The transition point moves to higher temperatures with increasing density as the matter becomes more saturated with antineutrinos at higher densities. Note that there are no transitions at the density $n_B = n_0$; in this case, the lepton decay is the dominant process in the whole range of the temperature $1 \leq T \leq 100$ MeV shown in Fig. 3.

To show the transition between the two regimes we plot the equilibration rates for neutron decay and lepton capture processes separately as functions of the scaled chemical potentials α_{ν_l} in Fig. 4. As seen from the figure, the curves representing the rates of the neutron decay and the lepton capture processes intersect at a value of the scaled chemical potential within the range $-5 \leq \alpha_{\nu_l} \leq -3$. Note that the regime of neutrino-dominated equilibration starts already around $\alpha_{\nu_l} \simeq -3$, where the antineutrino density is still

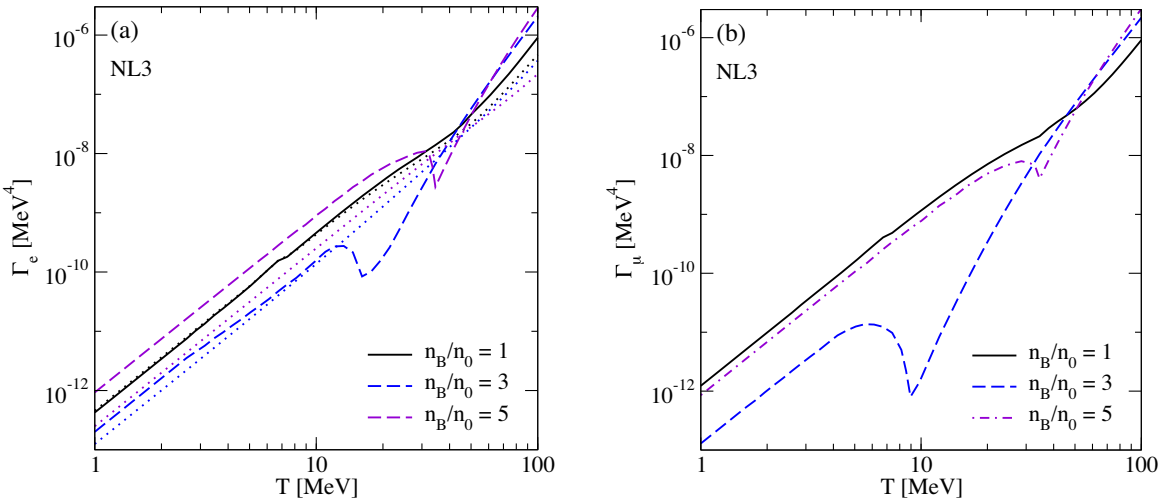

FIG. 3. The summed β-equilibration rates $\Gamma_l = \Gamma_{n\leftrightarrow pl\bar{\nu}} + \Gamma_{pl\leftrightarrow n\nu}$ for electronic (a) and muonic (b) Urca processes as functions of the temperature for various densities for the model NL3. In this case the dominant process is the neutron decay at low temperatures and the lepton capture at high temperatures. The dotted lines in panel (a) show the electron capture rates computed in Ref. [22] within the approximation of nonrelativistic nucleons.

higher than the neutrino density. The reason for this is the difference in the available phase space for the neutron decay and lepton capture processes. Indeed, the lepton capture process has a larger kinematic phase space than the neutron decay, therefore for equal densities of neutrinos and antineutrinos (i.e., at vanishing neutrino chemical potential) the neutron decay rates are suppressed as compared to the lepton decay rates.

As in the case of DDME2 model, we show also the nonrelativistic electron capture rates in panel (a) of Fig. 3. The nonrelativistic approximation underestimates the exact rates by factors from 1 to 10 in the regions away from the minimum, but close to the minimum, we have the opposite behavior: the exact relativistic rates are lower as there is no minimum in the nonrelativistic approximation (the transition between the antineutrino and neutrino-dominated regimes is smooth in the nonrelativistic approximation). We thus conclude that the sharp drop of the neutron decay rate and the minimum at the transition point is a purely relativistic effect and does not appear in the nonrelativistic treatment.

2. Rates of leptonic processes

Next we discuss the results of the leptonic process rates given by Eqs. (25)–(27). Figure 5 shows the neutrino (a) and the antineutrino (b) absorption rates for the model DDME2. As seen from panel (a), the neutrino absorption

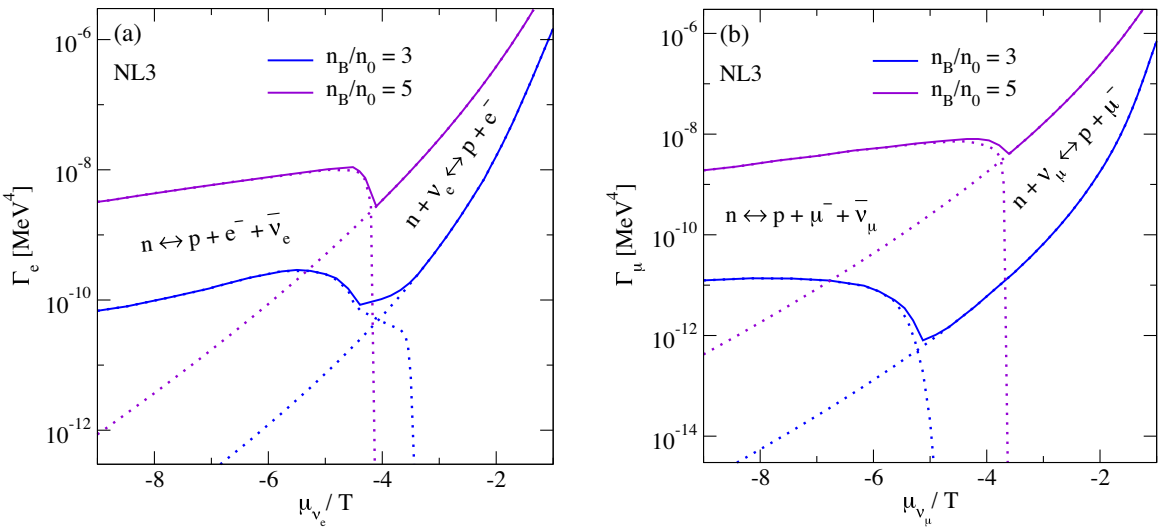

FIG. 4. The relative rates of neutron decay and lepton capture processes as functions of the scaled-to-temperature neutrino chemical potentials for electrons (a) and muons (b) for two values of the density for the model NL3.

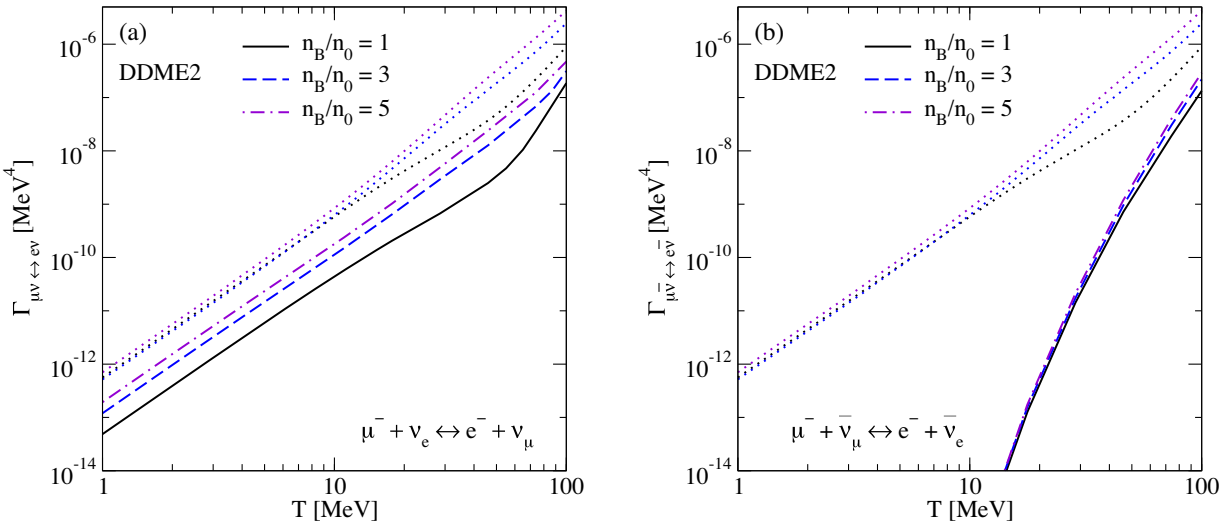

FIG. 5. Rates of leptonic β-equilibration processes as functions of the temperature for different values of the density for the model DDME2. The panel (a) refers to the neutrino absorption, and the panel (b) to the antineutrino absorption processes. We see that for DDME2 the leptonic rates are always at least an order of magnitude slower than the Urca electron capture rates (shown by the dotted lines for comparison; the muon capture rates are slightly higher than the electron capture rates and are not shown.).

rates show similar temperature dependence to the lepton capture rates (shown by dotted lines), but are smaller on average by an order of magnitude. The antineutrino absorption rates are always many orders of magnitude smaller than the neutrino absorption rates except in the very high-temperature domain. The rate of the muon decay process is negligible as compared to the neutrino and antineutrino absorption processes because of the very small scattering phase space. These rates are related to the rate coefficients λ_X in the rate equations in a simple way, $\lambda_X = \Gamma_X/T$ (See Eqs. (18) and (19); similar relations hold for the leptonic reactions since they have exactly the same kinematics.) We can therefore conclude that within the DDME2 model the leptonic processes are always much slower than the Urca processes, putting the material in the "slow lepton equilibration" regime.

In the NL3 model, the neutrino absorption is more efficient at low densities but is suppressed at high densities and low or moderate temperatures, see Fig. 6. The antineutrino absorption rates show the opposite behavior: they

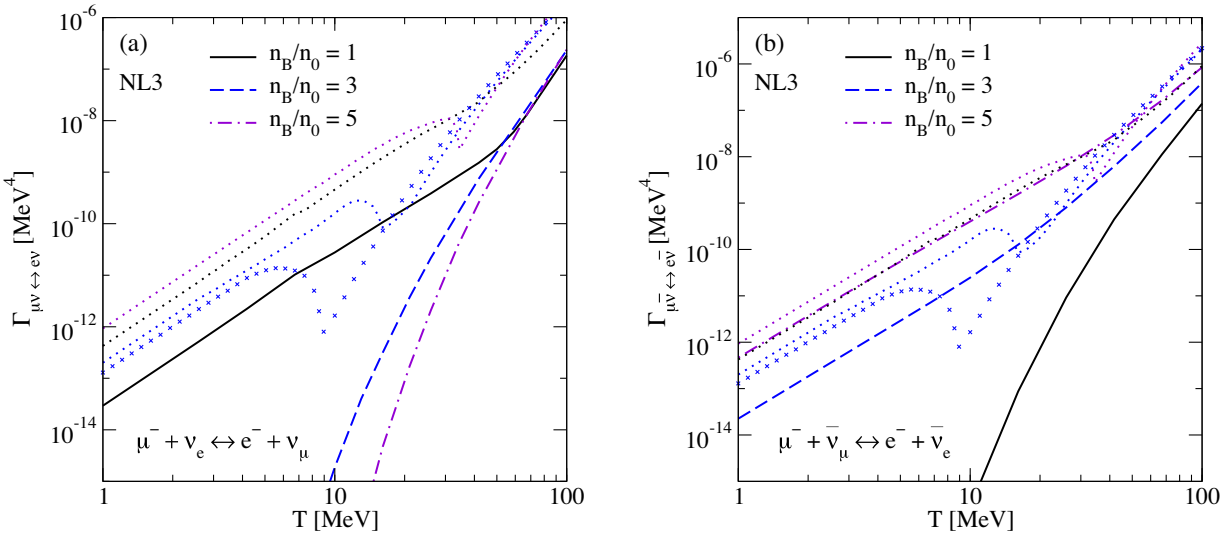

FIG. 6. Rates of leptonic β-equilibration processes as functions of the temperature for different values of the density for the model NL3. The panel (a) refers to the neutrino absorption, and the panel (b) to the antineutrino absorption processes. We see that for NL3 the leptonic rates are generally much slower than the summed Urca process rates $\Gamma_l \equiv \Gamma_{n\leftrightarrow pl\bar{\nu}} + \Gamma_{pl\leftrightarrow n\nu}$ (shown by the dotted lines for comparison for electrons; the muonic Urca process rates Γ_μ differ from Γ_e significantly only at the density $n_B = 3n_0$ and are shown by blue crosses) except near the transition point where the Urca rate goes through a minimum.

dominate the leptonic processes at high densities and are damped at low densities. However, the summed rate of leptonic processes in the case of NL3 model is qualitatively similar to those of the model DDME2. Consequently, as we see in Fig. 6, the material described by the NL3 model is almost always in the "slow lepton equilibration" regime. The only exception is the region around the transition point where the Urca process rate has a minimum. Note that the "fast lepton equilibration" regime is realized only around the minimum of the *muonic* Urca rates.

B. Bulk viscosity of relativistic *npe* matter

In this subsection we will neglect muons and discuss the bulk viscosity arising only from electronic Urca processes. We include relativistic corrections to the nucleon spectrum both in the equilibration rates and the nucleon susceptibilities. The bulk viscosity of $npe\nu_e$ matter is given by Eq. (91) with the susceptibilities C_1 and A_1 defined by Eqs. (88) and (54).

The susceptibility A_1 is not sensitive to the temperature and the density, whereas C_1 increases with density and typically crosses zero at a temperature-dependent value of the density where the proton fraction in β-equilibrated matter has a minimum as a function of the density. At this critical density, the system becomes scale-invariant, so compression does not drive the system out of equilibrium. This implies vanishing bulk viscosity at critical densities.

Figure 7 shows the susceptibility prefactor C_1^2/A_1 as a function of density for two values of the temperature. At the critical density, it drops to zero and slowly increases with the density above that point. For comparison we show also the results of our previous work [22] with the dotted lines, which were obtained with the nonrelativistic spectrum for nucleons. We see that the nonrelativistic approximation strongly overestimates the susceptibility even at low densities $n_B \leq 2n_0$ where the relativistic corrections to the nucleonic spectrum are relatively small.

The beta relaxation rates $\gamma_e = \lambda_e A_1$ of electronic Urca processes which determine the location of the resonant maximum of the bulk viscosity are shown in Fig. 8. Qualitatively γ_e closely follows the behavior of Γ_e. As the typical frequencies of density oscillations in neutron star mergers are several kHz, the relaxation is always fast, $\gamma_e \gg \omega$ (1 kHz corresponds to 4.14×10^{-18} MeV). Thus, the neutrino-trapped matter is in the fast equilibration regime, and from (91) the bulk viscosity is independent of the oscillation frequency and is given by $\zeta = C_1^2/(A_1\gamma_e)$.

The results of the bulk viscosity arising from electronic Urca processes are shown in Fig. 9. At low temperatures, $T \leq 10$ MeV the bulk viscosity decreases according to the scaling $\zeta_e \sim T^{-2}$, which breaks down at higher temperatures where the system approaches the point of scale-invariance. In the case of NL3 model, the bulk viscosity has a local maximum at high densities due to the transition from the antineutrino-dominated regime to the neutrino-dominated regime. At that maximum, the bulk viscosity jumps nearly by an order of magnitude. Comparing these results with ones obtained within the nonrelativistic approximation for nucleons we see that the bulk viscosity decreases by orders of magnitude when the relativistic corrections are properly taken into account. The main reason for this is much lower susceptibility C_1 as compared to the nonrelativistic case, and also the higher β-equilibration rates. We also observe that the local maxima in the case of NL3 model appear only in full relativistic computation as was mentioned above.

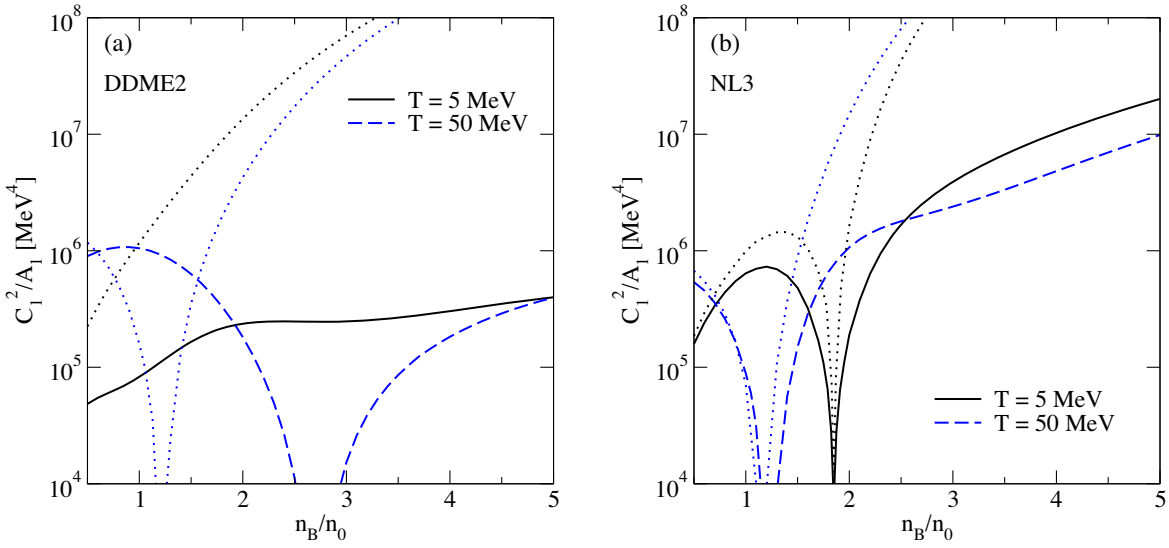

FIG. 7. The susceptibility prefactor C_1^2/A_1 as a function of the baryon density for two values of the temperature for (a) model DDME2 and (b) model NL3. The dotted lines show the nonrelativistic results used in Ref. [22].

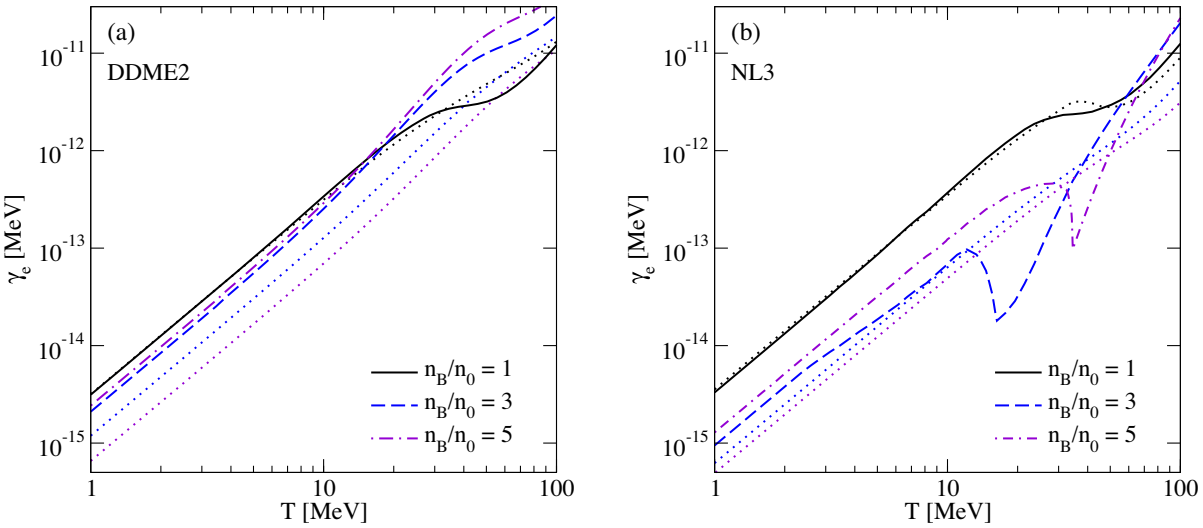

FIG. 8. The relaxation rate γ_e as a function of the temperature for fixed values of the density for (a) model DDME2; (b) model NL3. The dotted lines show the relaxation rates computed in Ref. [22] using the approximation of nonrelativistic nucleons. Typical density oscillations in mergers are at $\omega \sim 1$ kHz $\approx 4 \times 10^{-18}$ MeV, so neutrino-trapped matter is always in the fast equilibration regime.

C. Bulk viscosity of relativistic *npeμ* matter

In this section, we present the results of the bulk viscosity of nuclear matter including the contribution of a muonic component. As discussed in Sec. IV A, in the case of the DDME2 model the rates of the leptonic processes are much smaller than the rates of the Urca processes, see Fig. 5. Therefore, the bulk viscosity of $npe\mu$ matter can be computed according to the slow lepton-equilibration limit, as discussed in Sec. III. As the equilibration rates are much larger than the oscillation frequency, the bulk viscosity for the DDME2 model can be computed from Eq. (93). The results are shown in the left panel of Fig. 10. The generic behavior of the bulk viscosity of $npe\mu$ matter is similar to the one of npe matter but the former exceeds the latter by factors from 3 to 10 at the left side of the minimum. Above the minimum, the bulk viscosity of $npe\mu$ matter is almost the same as the bulk viscosity of npe matter. However, there is an important difference in the high-temperature regime, where the total bulk viscosity has a sharp minimum but does not drop to zero, as it was the case of the bulk viscosity of npe matter. This behavior is easy to understand by noting that in the relevant temperature-density range we have mainly $(A_n + A_p)C_1 \ll A_1 C_2$, $(A_n + A_p)C_2 \ll A_2 C_1$, $(A_n + A_p)^2 \ll A_1 A_2$, which allows to simplify Eq. (93) to

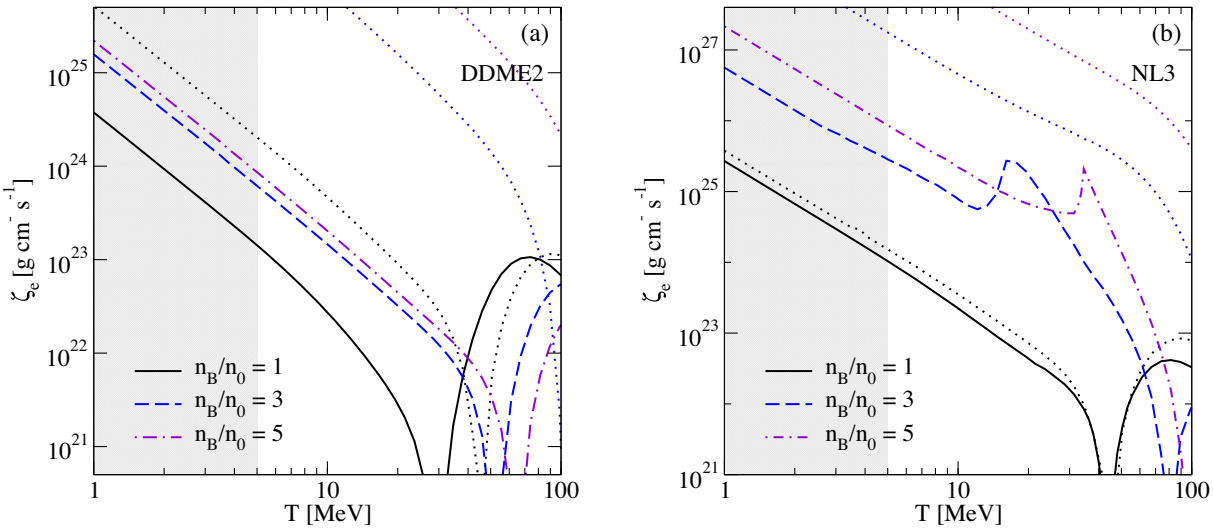

FIG. 9. The bulk viscosity due to electron Urca processes as a function of the temperature for (a) model DDME2; (b) model NL3. The region $T \leq 5$ MeV is shaded because neutrinos are no longer trapped at those temperatures. The dotted lines show the results of Ref. [22] using the approximation of nonrelativistic nucleons.

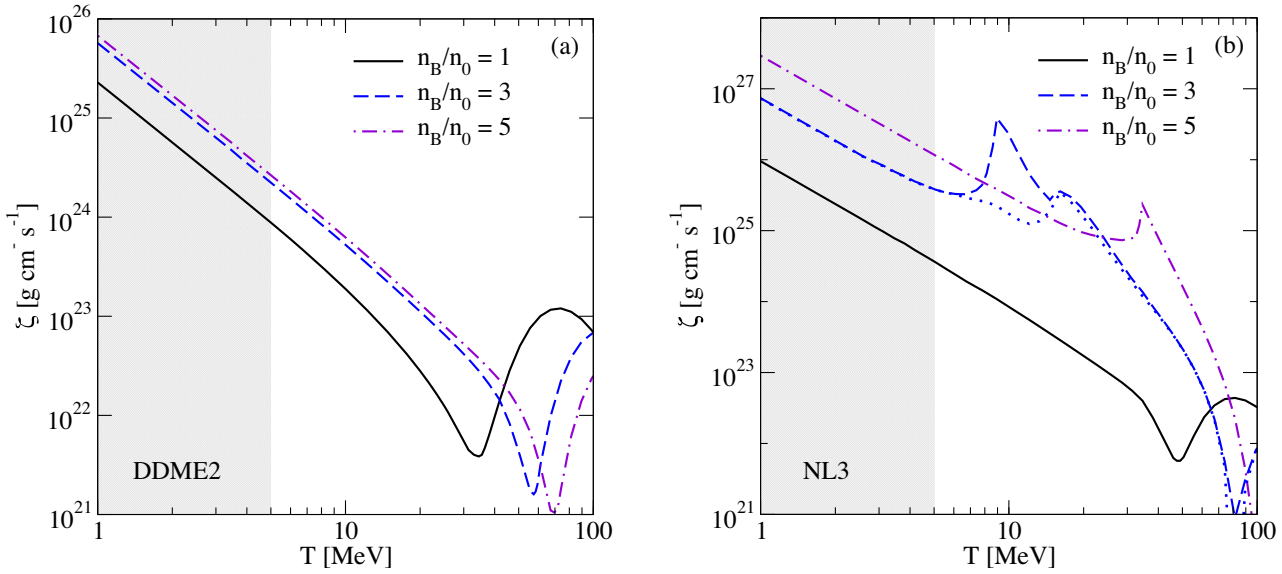

FIG. 10. The bulk viscosity of neutrino-trapped $npe\mu$ matter as a function of the temperature for (a) model DDME2; (b) model NL3. The region $T \leq 5$ MeV is shaded because neutrinos are no longer trapped at those temperatures. All curves assume the slow lepton-equilibration regime except the dotted line in panel (b) which assumes fast lepton equilibration.

$$\zeta \simeq \frac{\lambda_e (A_1 C_2)^2 + \lambda_\mu (A_2 C_1)^2}{\lambda_e \lambda_\mu (A_1 A_2)^2} = \frac{C_2^2}{\lambda_\mu A_2^2} + \frac{C_1^2}{\lambda_e A_1^2} = \zeta_e + \zeta_\mu, \tag{94}$$

where ζ_e and ζ_μ are the partial contributions of electronic and muonic Urca processes, respectively, to the bulk viscosity. Both susceptibilities C_1 and C_2 cross zero at high temperatures, but the values of those critical temperatures for C_1 and C_2 are slightly shifted from each other. As a result, the summed ζ has a minimum at a temperature that lies between these two temperatures but does not drop to zero.

Turning to the NL3 model we note that also in this case the matter is mainly in the slow lepton-equilibration regime except for the region close to the minimum of equilibration rates, where for $n_B/n_0 = 3$ and $n_B/n_0 = 5$ we have the opposite regime of fast lepton-equilibration, see Fig. 6. Figure 10, panel (b) therefore shows the bulk viscosity in the slow lepton-equilibration limit by the solid, dashed and the dashed-dotted lines. The one exception is the dotted line, which shows the fast lepton equilibration limit [Eq. (70)] for $n_B/n_0 = 3$.

At the highest density, $n_B/n_0 = 5$, the bulk viscosity has one local maximum as the electronic and muonic Urca process rates have minima at almost the same temperature, see Fig. 3. For moderate density $n_B/n_0 = 3$ the minima of Urca process rates for electrons and muons are at different temperatures, therefore the bulk viscosity has local maxima at both temperatures. However, near the maxima we cannot rely on the slow lepton equilibration approximation: in the fast lepton-equilibration limit (dotted line) the first maximum is eliminated by leptonic processes, whereas the second maximum remains. At the highest density $n_B/n_0 = 5$, the numerical results for the bulk viscosity in the fast lepton-equilibration limit are found to be very close to those of slow lepton-equilibration limit and are not shown on the figure.

The structure of the postmerger object changes with time from initially having double density-peaks, associated with the two neutron stars, to a single density-peak structure corresponding to the remnant (see, for example, Refs. [5–16]). So far, we consider the variations of the bulk viscosity at fixed density, which corresponds to moving along the constant density surfaces in such an object. It is also interesting to consider the isothermal surfaces along which the density is changing. The temperature evolution in the post-merger object replicates that of the density, i.e., a double peak high-temperature structure evolves in time into a single peak structure. To account for this type of variation, we plot the bulk viscosity as a function of the density in Fig. 11.

The density variations of bulk viscosity for each value of temperature represent self-similar curves, which are shifted with respect to each other by a magnitude which depends on the change in the temperature. In the case of model NL3 the curves $T = 5$, 30, 50 MeV correspond to the slow lepton-equilibration limit, and only the curve $T = 10$ MeV shows the results of the fast equilibration regime.

D. Damping of density oscillations

In this last subsection, we estimate the timescales of bulk viscous damping of density oscillations in neutrino-trapped $npe\mu$ matter. The characteristic timescale of damping of density oscillations is given by [20,21,24]

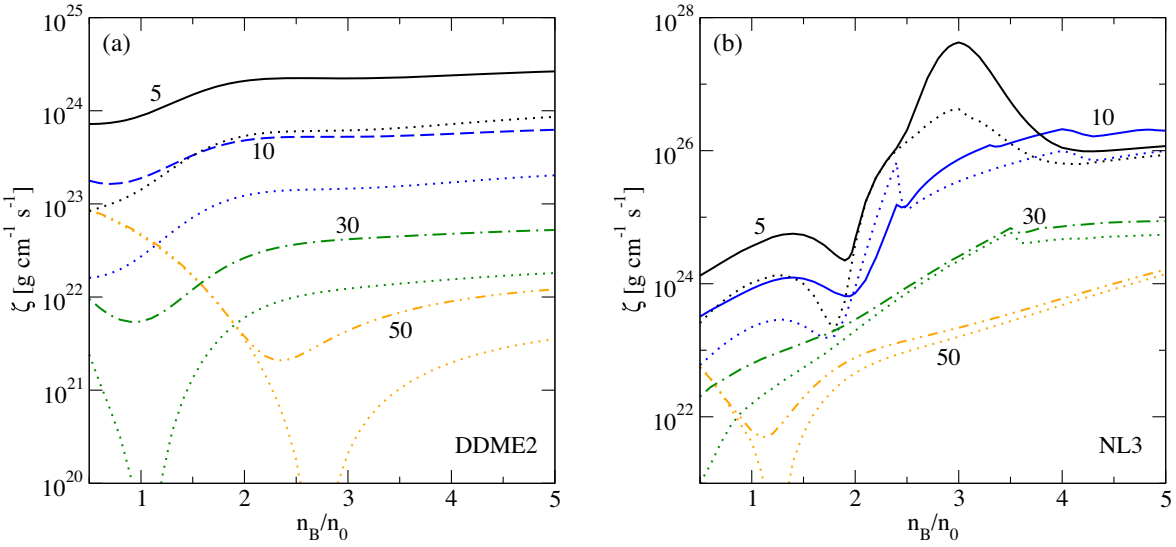

FIG. 11. The bulk viscosity of neutrino-trapped $npe\mu$ matter as a function of the density for various temperatures indicated on the plot for (a) model DDME2; (b) model NL3. The dotted curves show the corresponding bulk viscosities of npe matter.

$$\tau_\zeta = \frac{1}{9}\frac{Kn_B}{\omega^2\zeta}, \tag{95}$$

where

$$K = 9n_B\frac{\partial^2\varepsilon}{\partial n_B^2} \tag{96}$$

is the (isothermal) incompressibility of nuclear matter. The incompressibility of nuclear matter at finite temperatures is shown in Ref. [24].

As the bulk viscosity is independent of the oscillation frequency, the damping timescale is inversely proportional to the square of ω. We show τ_ζ as a function of the temperature in Fig. 12 for $f = 10$ kHz. The nuclear incompressibility is almost independent of the temperature. Therefore the damping timescale as a function of the temperature closely follows the inverse bulk viscosity showing sharp maxima in the high-temperature regime. In the case of NL3 model there are local minima resulting from the transition of the matter from the antineutrino-dominated regime to the neutrino dominated regime. However, the damping timescales in the neutrino/antineutrino trapped regime exceeds the characteristic timescales for the long-term postmerger evolution timescale $\lesssim 1$ s at temperatures above 5 MeV. At lower frequencies, the damping timescales will be even larger. Thus, we conclude that the

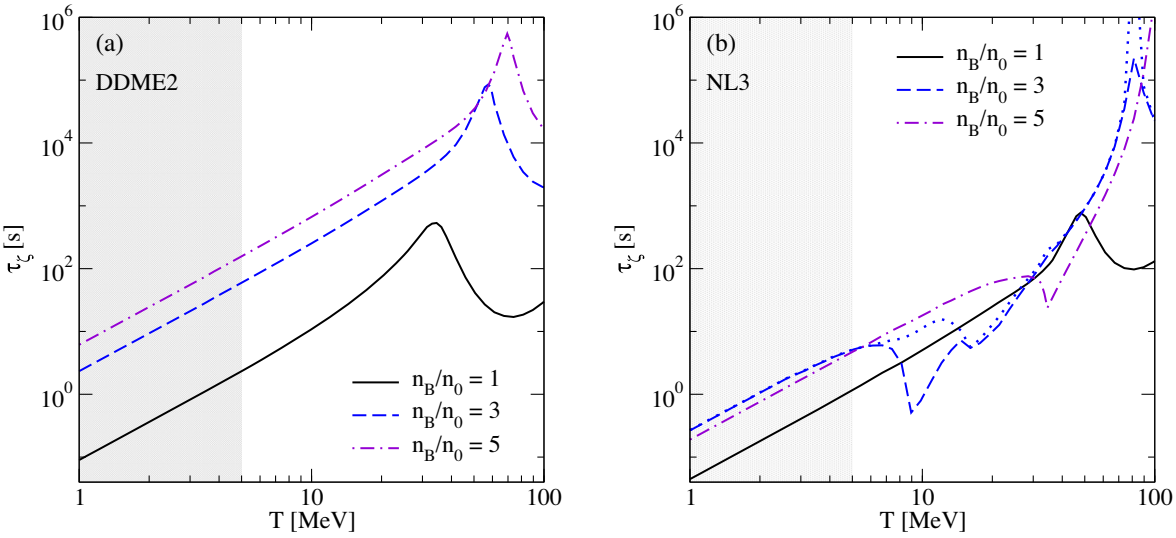

FIG. 12. The oscillation damping timescale as a function of temperature for various densities and for frequency fixed at $f = 10$ kHz for (a) model DDME2; (b) model NL3. The result for the density $n_B/n_0 = 3$ in panel (b) should be replaced by the blue dotted line around the minimum.

bulk viscosity of neutrino-trapped $npe\mu$ matter from the Urca processes is not sufficiently large to affect the evolution of binary neutron-star mergers in the initial hot regime and could have an impact close to the neutrino untrapping temperature ~ 5 MeV.

V. CONCLUSIONS

In this work, we studied the bulk viscosity of neutrino-trapped $npe\mu$ matter from Urca processes under the conditions relevant to binary neutron star mergers. We first generalized the computation of the rates of relevant β-equilibration processes (i.e., the neutron decay and lepton capture) as well as those of relevant susceptibilities performed in Ref. [22] to include the relativistic corrections to the nucleonic spectra. We find that these corrections enhance the equilibration rates by factors from 1 to 10. The numerical computations were carried out within the relativistic density functional theory for two different EoS models of nuclear matter.

An interesting feature of full relativistic rates is their strong dependence on the scaled-to-temperature neutrino chemical potential α_{ν_l}. It turns out that if $\alpha_{\nu_l} \geq -3$ then the neutron decay rate is Boltzmann-suppressed, and the only equilibration process is the lepton capture. This is the case for DDME2 model which has a composition where the net neutrino densities are mainly positive in the relevant density-temperature range. The picture is quite different in the case of model NL3 where the net neutrino densities are positive only in the low temperature and low-density sector, and the antineutrino population increases with both density and temperature. At low densities and high temperatures, the lepton capture dominates as in the case of DDME2 model, but in the low-temperature and high-density domain, we have the opposite limit. Here the antineutrino population is dominant, and the neutron decay is the main equilibration process as long as $\alpha_{\nu_l} \leq -6$. For intermediate values $-6 \leq \alpha_{\nu_l} \leq -3$ both processes are important, and there is a transition point at around $\alpha_{\nu_l} \simeq (-5)$ to (-4) where the rates of neutron decay and lepton capture become equal. Close to this point the net equilibration rate has a sharp minimum.

The relativistic susceptibilities are found to be significantly (up to orders of magnitude) smaller than their corresponding nonrelativistic counterparts at densities $n_B/n_0 \geq 2$. Similar to the nonrelativistic case we find that the susceptibilities corresponding to the partial bulk viscosities from electronic and muonic Urca processes vanish at a critical density where the electron/muon fraction has a local minimum as a function of density at high temperatures $T \gtrsim 30$ MeV. At that point the system becomes scale-invariant: there is no chemical reequilibration induced by compression which implies zero bulk viscosity on the time scales relevant to mergers.

Neutrino-trapped matter is always in the regime of fast β-equilibration, i.e., the relaxation rates are much higher than the typical frequencies of density oscillations. As a result, the bulk viscosity is independent of the frequency and decreases with the temperature. This decrease is followed by sharp drops to zero at the points where the system becomes scale-invariant. In the case of model NL3 the bulk viscosity shows also local maxima at intermediate temperatures where the transition between the antineutrino- and neutrino-dominated regimes occurs.

The proper inclusion of muons in the computation of bulk viscosity requires analysis of relative rates of Urca processes and the rates of pure leptonic processes, i.e., muon decay, and neutrino/antineutrino absorption. We find that the rates of the leptonic reactions are slower than the Urca process rates almost in the entire temperature-density range. An exception occurs only in the narrow vicinity of the transition point in the case of NL3 model. We, therefore, conclude that the bulk viscosity of $npe\mu$ matter can typically be computed in the slow lepton-equilibration limit. The numerical results show that the bulk viscosity is enhanced by factors from 1 to 10 as compared to the viscosity of npe matter. Note that our study neglects so far the neutrino flavor conversion, which can affect our results. We plan to address this issue in a separate study.

Our estimates of the damping timescales of the density oscillations show that the bulk viscosity of relativistic $npe\mu$ matter in the neutrino-trapped regime is not an important source of damping of density oscillations over characteristic time-scales of neutron star mergers. However, long-lived remnants of mergers, which do not collapse to a black hole, can experience bulk viscous dissipation. Young protoneutron stars formed in supernova explosions offer another setting where the bulk viscosity of hot stellar matter could be important for assessing their oscillation spectrum and damping time scales.

We finally note that, the methods applied here can be used to obtain other microscopic characteristics of dense matter, such as, for example, neutrino opacities. The fully relativistic treatment of the rates should be of interest in a broader context of radiation and transport in thermal quantum field theories with applications to a wide range of relativistic systems.

ACKNOWLEDGMENTS

M. A. is supported by the U.S. Department of Energy, Office of Science, Office of Nuclear Physics under Award No. DE-FG02-05ER41375. The research of A. H. and A. S. was funded by the Volkswagen Foundation (Hannover, Germany) Grant No. 96 839. They acknowledge the support of the European COST Action "PHAROS" (CA16214). A. S. acknowledges the support by the Deutsche Forschungsgemeinschaft (DFG) Grant No. SE 1836/5-1. He also acknowledges the support of the Polish NCN Grant No. 2020/37/B/ST9/01937 at Wrocław University.

APPENDIX A: PHASE SPACE INTEGRALS

Here we extend the technique of computing the phase-space integrals discussed in [21,22] to fully relativistic case. Substituting the matrix element of the Urca process (10) into the rates (8) and the *inverse of* (9) and introducing a "dummy" integration [we use the same the mapping between the particles and their momenta $(l) \to k$, $(\nu_l/\bar{\nu}_l) \to k'$, $(p) \to p$, and $(n) \to p'$ as before] we obtain

$$\Gamma_{n\to pl\bar{\nu}}(\mu_{\Delta_l}) = 2G^2 \int d^4q \int \frac{d^3p}{(2\pi)^3 p_0} \int \frac{d^3p'}{(2\pi)^3 p_0'} \int \frac{d^3k}{(2\pi)^3 k_0} \int \frac{d^3k'}{(2\pi)^3 k_0'} (k\cdot p)(k'\cdot p') \times \bar{f}(k)\bar{f}(p)\bar{f}(k')f(p')(2\pi)^4\delta^{(4)}(k+p-q)\delta^{(4)}(k'-p'+q) = 2G^2 \int d^4q I_1(q) I_2(q), \tag{A1}$$

$$\Gamma_{n\nu\to pl}(\mu_{\Delta_l}) = 2G^2 \int d^4q \int \frac{d^3p}{(2\pi)^3 p_0} \int \frac{d^3p'}{(2\pi)^3 p_0'} \int \frac{d^3k}{(2\pi)^3 k_0} \int \frac{d^3k'}{(2\pi)^3 k_0'} (k\cdot p)(k'\cdot p') \times \bar{f}(k)\bar{f}(p)f(k')f(p')(2\pi)^4\delta^{(4)}(k+p-q)\delta^{(4)}(-k'-p'+q) = 2G^2 \int d^4q I_1(q) I_3(q), \tag{A2}$$

where

$$I_1(q) = \int \frac{d^3p}{(2\pi)^3 p_0} \int \frac{d^3k}{(2\pi)^3 k_0} \bar{f}(k)\bar{f}(p)(k\cdot p)(2\pi)^4\delta^{(4)}(k+p-q), \tag{A3}$$

$$I_2(q) = \int \frac{d^3p'}{(2\pi)^3 p_0'} \int \frac{d^3k'}{(2\pi)^3 k_0'} \bar{f}(k')f(p')(k'\cdot p')\delta^{(4)}(k'-p'+q), \tag{A4}$$

$$I_3(q) = \int \frac{d^3p'}{(2\pi)^3 p_0'} \int \frac{d^3k'}{(2\pi)^3 k_0'} f(k')f(p')(k'\cdot p')\delta^{(4)}(-k'-p'+q), \tag{A5}$$

with $\delta^{(4)}(k+p-q) = \delta(\boldsymbol{k}+\boldsymbol{p}-\boldsymbol{q})\delta(\epsilon_k+\epsilon_p-\omega-\mu_{\Delta_l})$, and $\delta^{(4)}(\pm k'-p'+q) = \delta(\pm\boldsymbol{k}'-\boldsymbol{p}'+\boldsymbol{q})\delta(\pm\epsilon_{k'}-\epsilon_{p'}+\omega)$. Here the energy conservation δ-function has been transformed according to $\delta(k_0+p_0\pm k_0'-p_0') = \delta(\epsilon_l+\epsilon_p-\epsilon_n\pm\epsilon_{\bar{\nu}_l/\nu_l}-\mu_{\Delta_l})$, where we added and subtracted μ_{Δ_l} in the argument of the δ-function, and denoted by ϵ_i the energies of the particles computed from their (effective) chemical potentials, e.g., $\epsilon_p = \sqrt{p^2+m_p^{*2}}-\mu_p^*$. Since the rates of the inverse processes can be obtained by interchanging in Eqs. (A1) and (A2) $f(p_i) \leftrightarrow \bar{f}(p_i)$ for all particles, the problem reduces to the computation of three q-dependent integrals $I_1(q)$, $I_2(q)$ and $I_3(q)$ given by Eqs. (A3)–(A5).

To compute the integral $I_1(q)$ we integrate over proton momentum and separate the angular part of the remaining integral, which gives

$$I_1(q) = (2\pi)^{-1} \int_{m_l}^{\infty} \frac{k dk_0}{p_0} \bar{f}(\epsilon_k)\bar{f}(\bar{\omega}-\epsilon_k) \int_{-1}^{1} dx(\bar{\omega}'k_0 - qkx - m_l^2)\delta(\epsilon_k+\epsilon_{q-k}-\bar{\omega}), \tag{A6}$$

where $\bar{\omega} = \omega+\mu_{\Delta_l}$, $\bar{\omega}' = \bar{\omega}+\mu_p^*+\mu_l$, and x is the cosine of the angle between $\boldsymbol{k}$ and $\boldsymbol{q}$. The angular integral is done by using the δ-function to obtain [recall that $\bar{f}(\epsilon) = f(-\epsilon)$]

$$I_1(q) = \frac{1}{4\pi q}[(\mu_l+\mu_p^*+\bar{\omega})^2 - m_l^2 - m_p^{*2} - q^2] \int_{m_l-\mu_l}^{\mu_p^*+\bar{\omega}} d\epsilon_k \bar{f}(\epsilon_k) f(\epsilon_k-\bar{\omega})\theta(1-|x_0|), \tag{A7}$$

where x_0 is the zero of the argument of the δ-function

$$x_0 = \frac{1}{2kq}[-(\epsilon_k-\mu_p^*-\bar{\omega})^2 + m_p^{*2} + k^2 + q^2], \tag{A8}$$

and the limits of integration are found from the limits on the lepton energy ϵ_k

$$(k-q)^2+m_p^{*2}\le(\epsilon_k-\mu_p^*-\bar{\omega})^2\le(k+q)^2+m_p^{*2}. \tag{A9}$$

The energy integral in Eq. (A7) could be done analytically, but for numerical implementation, the form given above is more suitable.

The computation of the remaining integrals proceeds in full analogy to the above. For integral $I_2(q)$ we find

$$I_2(q)=\frac{1}{2(2\pi)^5 q}[-(\mu_{\nu_l}+\mu_n^*+\omega)^2+m_{\nu_l}^2+m_n^{*2}+q^2]\int_{m_{\nu_l}+\mu_{\nu_l}}^{\infty}d\epsilon_{k'}\,\bar{f}(\epsilon_{k'})f(\epsilon_{k'}+\omega)\theta(1-|y_0|), \tag{A10}$$

where y_0 is the zero of the argument of the δ-function, i.e.,

$$y_0=\frac{1}{2k'q}[(\epsilon_{k'}+\mu_n^*+\omega)^2-m_n^{*2}-k'^2-q^2], \tag{A11}$$

and the step-function sets the following limits on the neutrino energy $\epsilon_{k'}$

$$(k'-q)^2+m_n^{*2}\le(\epsilon_{k'}+\mu_n^*+\omega)^2\le(k'+q)^2+m_n^{*2}. \tag{A12}$$

For the integral $I_3(q)$ we find

$$I_3(q)=\frac{1}{2(2\pi)^5 q}[(\mu_{\nu_l}+\mu_n^*+\omega)^2-m_{\nu_l}^2-m_n^{*2}-q^2]\int_{m_{\nu_l}-\mu_{\nu_l}}^{\omega+\mu_n^*}d\epsilon_{k'}\,f(\epsilon_{k'})\bar{f}(\epsilon_{k'}-\omega)\theta(1-|z_0|), \tag{A13}$$

where z_0 is the zero of the argument of the δ-function, i.e.,

$$z_0=\frac{1}{2k'q}[-(\epsilon_{k'}-\mu_n^*-\omega)^2+m_n^{*2}+k'^2+q^2], \tag{A14}$$

and the step-function sets the following limits on the neutrino energy $\epsilon_{k'}$

$$(k'-q)^2+m_n^{*2}\le(\epsilon_{k'}-\mu_n^*-\omega)^2\le(k'+q)^2+m_n^{*2}. \tag{A15}$$

The expressions for the integrals (A7), (A10) and (A13) are slightly more general than used in the main body of the text because they include the nonzero mass of neutrinos. As we do not consider neutrino oscillations they can be neglected hereafter, i.e., we put $m_{\nu_l}=0$. Combining Eqs. (A1), (A2), (A7), (A10) and (A13), we obtain the final expressions (13) and (14) of the main text.

Now we are in a position to compute the derivatives of $\Gamma_{n\to pl\bar{\nu}}$ and $\Gamma_{pl\to n\nu}$ with respect to μ_{Δ_l}. Note that only the integral I_1 depends on μ_{Δ_l}, and, exploiting the following identity between the Fermi and Bose functions

$$\bar{f}(z)f(z-y)=g(-y)[f(z)-f(z-y)], \tag{A16}$$

from Eq. (A7) we obtain

$$\frac{\partial I_1}{\partial\mu_{\Delta_l}}=\frac{1+g(\bar{\omega})}{4\pi qT}\left[g(\bar{\omega})\Lambda_1(\bar{\omega})-T\frac{\partial}{\partial\bar{\omega}}\Lambda_1(\bar{\omega})\right], \tag{A17}$$

where

$$\Lambda_1(\bar{\omega})=[(\mu_l+\mu_p^*+\bar{\omega})^2-m_l^2-m_p^{*2}-q^2]\int_{m_l-\mu_l}^{\mu_p^*+\bar{\omega}}d\epsilon_k[f(\epsilon_k)-f(\epsilon_k-\bar{\omega})]\theta(1-|x_0|). \tag{A18}$$

The rate derivatives then take the form

$$\frac{\partial}{\partial\mu_{\Delta_l}}\Gamma_{n\to pl\bar{\nu}}(\mu_{\Delta_l})=-\frac{G^2}{(2\pi)^5T}\int_{-\infty}^{\infty}d\omega\int_0^{\infty}dq\,g(\omega)[1+g(\bar{\omega})]\left[g(\bar{\omega})\Lambda_1(\bar{\omega})-T\frac{\partial}{\partial\bar{\omega}}\Lambda_1(\bar{\omega})\right]\Lambda_2(\omega), \tag{A19}$$

$$\frac{\partial}{\partial\mu_{\Delta_l}}\Gamma_{n\nu\to pl}(\mu_{\Delta_l}) = -\frac{G^2}{(2\pi)^5 T}\int_{-\infty}^{\infty} d\omega \int_0^{\infty} dq\, g(\omega)[1+g(\bar{\omega})]\left[g(\bar{\omega})\Lambda_1(\bar{\omega}) - T\frac{\partial}{\partial\bar{\omega}}\Lambda_1(\bar{\omega})\right]\Lambda_3(\omega), \tag{A20}$$

where

$$\Lambda_2(\omega) = [(\mu_{\nu_l}+\mu_n^*+\omega)^2 - m_{\nu_l}^2 - m_n^{*2} - q^2]\int_{m_{\nu_l}+\mu_{\nu_l}}^{\infty} d\epsilon_{k'}[f(\epsilon_{k'}) - f(\epsilon_{k'}+\omega)]\theta(1-|y_0|), \tag{A21}$$

$$\Lambda_3(\omega) = [(\mu_{\nu_l}+\mu_n^*+\omega)^2 - m_{\nu_l}^2 - m_n^{*2} - q^2]\int_{m_{\nu_l}-\mu_{\nu_l}}^{\omega+\mu_n^*} d\epsilon_{k'}[f(\epsilon_{k'}) - f(\epsilon_{k'}-\omega)]\theta(1-|z_0|). \tag{A22}$$

The derivatives of the inverse rates can be obtained by replacing $g(\omega)\to 1+g(\omega)$, $g(\bar{\omega})\leftrightarrow 1+g(\bar{\omega})$ in Eqs. (A19) and (A20). For the λ–coefficients we obtain

$$\lambda_{n\leftrightarrow pl\bar{\nu}} = \frac{G^2}{(2\pi)^5 T}\int_{-\infty}^{\infty} d\omega \int_0^{\infty} dq\left\{g(\bar{\omega})[1+g(\bar{\omega})]\Lambda_1(\bar{\omega}) + [g(\omega)-g(\bar{\omega})]T\frac{\partial}{\partial\bar{\omega}}\Lambda_1(\bar{\omega})\right\}\Lambda_2(\omega), \tag{A23}$$

$$\lambda_{pl\leftrightarrow n\nu} = \frac{G^2}{(2\pi)^5 T}\int_{-\infty}^{\infty} d\omega \int_0^{\infty} dq\left\{g(\bar{\omega})[1+g(\bar{\omega})]\Lambda_1(\bar{\omega}) + [g(\omega)-g(\bar{\omega})]T\frac{\partial}{\partial\bar{\omega}}\Lambda_1(\bar{\omega})\right\}\Lambda_3(\omega). \tag{A24}$$

In β-equilibrium $\bar{\omega}=\omega$ which along with the relations $I_1 = -[1+g(\bar{\omega})]\Lambda_1(\bar{\omega})$, $I_2 = -g(\omega)\Lambda_2(\omega)$, $I_3 = -g(\omega)\Lambda_3(\omega)$ leads to Eqs. (18) and (19) of the main text.

1. Low-T limit of Urca process rates

In the limit of low temperature the inequalities (A9), (A12) and (A15) reduce to

$$\theta_x = \theta(p_{Fl}+p_{Fp}-q)\theta(q-|p_{Fl}-p_{Fp}|), \tag{A25}$$

$$\theta_y = \theta(p_{F\nu_l}+p_{Fn}-q)\theta(q-|p_{F\nu_l}-p_{Fn}|), \tag{A26}$$

$$\theta_z = \theta(p_{F\nu_l}+p_{Fn}-q)\theta(q-|p_{F\nu_l}-p_{Fn}|), \tag{A27}$$

where we used the notations θ_x, θ_y and θ_z introduced in Eqs. (13) and (14). Then the integrals (A7), (A10) and (A13) (in β-equilibrium) can be approximated as

$$\begin{aligned} I_1(q) &\simeq \frac{g(-\omega)}{4\pi q}[(\mu_l+\mu_p^*)^2 - m_l^2 - m_p^{*2} - q^2]\theta_x\int_{m_l-\mu_l}^{\mu_p^*+\omega} d\epsilon_k[f(\epsilon_k) - f(\epsilon_k-\omega)] \\ &\simeq -\frac{\omega g(-\omega)}{4\pi q}\theta_x(p_{Fp}^2 + p_{Fl}^2 + 2\mu_l\mu_p^* - q^2), \end{aligned} \tag{A28}$$

$$\begin{aligned} I_2(q) &\simeq \frac{g(\omega)}{2(2\pi)^5 q}[-(\mu_{\nu_l}+\mu_n^*)^2 + m_{\nu_l}^2 + m_n^{*2} + q^2]\theta_y\int_{m_{\nu_l}+\mu_{\nu_l}}^{\infty} d\epsilon_{k'}[f(\epsilon_{k'}) - f(\epsilon_{k'}+\omega)] \\ &\simeq -\frac{g(\omega)T}{2(2\pi)^5 q}\theta_y(p_{F\nu_l}^2 + p_{Fn}^2 + 2\mu_{\nu_l}\mu_n^* - q^2)\ln\left|\frac{1+\exp(-\frac{m_{\nu_l}+\mu_{\nu_l}}{T})}{1+\exp(-\frac{m_{\nu_l}+\mu_{\nu_l}+\omega}{T})}\right|, \end{aligned} \tag{A29}$$

$$\begin{aligned} I_3(q) &\simeq \frac{g(\omega)}{2(2\pi)^5 q}[(\mu_{\nu_l}+\mu_n^*)^2 - m_{\nu_l}^2 - m_n^{*2} - q^2]\theta_z\int_{m_{\nu_l}-\mu_{\nu_l}}^{\omega+\mu_n^*} d\epsilon_{k'}[f(\epsilon_{k'}-\omega) - f(\epsilon_{k'})] \\ &\simeq -\frac{g(\omega)T}{2(2\pi)^5 q}\theta_z(p_{Fn}^2 + p_{F\nu_l}^2 + 2\mu_{\nu_l}\mu_n^* - q^2)\ln\left|\frac{1+\exp(-\frac{m_{\nu_l}-\mu_{\nu_l}}{T})}{1+\exp(-\frac{m_{\nu_l}-\mu_{\nu_l}-\omega}{T})}\right|. \end{aligned} \tag{A30}$$

Note that in $I_1(q)$ the integral is approximated as ω because baryons are highly degenerate; in the remaining integrals, the logarithmic factor should be kept since neutrinos are thermal. In the low-temperature neutrino-trapped matter $\mu_{\nu_l}/T\to\infty$,

which implies $I_2 = 0$ and $\Gamma_{n\leftrightarrow pl\bar{\nu}} = 0$. In this case the logarithm in Eq. (A30) is $-\omega/T$, and for $\Gamma_{pl\leftrightarrow n\nu}$ from Eqs. (A2) we find (we put again $m_{\nu_l} = 0$)

$$\begin{aligned}\Gamma_{pl\leftrightarrow n\nu} &= -2G^2 4\pi \int_{-\infty}^{\infty} d\omega\omega^2 \int_0^{\infty} q^2 dq \frac{g(-\omega)}{4\pi q}\theta(p_{Fl}+p_{Fp}-q)\theta(q-|p_{Fl}-p_{Fp}|)(p_{Fp}^2+p_{Fl}^2+2\mu_l\mu_p^*-q^2)\\ &\times \frac{g(\omega)}{2(2\pi)^5 q}\theta(p_{F\nu_l}+p_{Fn}-q)\theta(q-|p_{F\nu_l}-p_{Fn}|)(p_{Fn}^2+p_{F\nu_l}^2+2\mu_{\nu_l}\mu_n^*-q^2)\\ &= \frac{G^2T^3}{48\pi^3}\left\{\frac{(p_{Fl}+p_{Fp})^5-(p_{Fn}-p_{F\nu_l})^5}{5}-\frac{(p_{Fl}+p_{Fp})^3-(p_{Fn}-p_{F\nu_l})^3}{3}\right.\\ &\times (p_{Fp}^2+p_{Fl}^2+2\mu_l\mu_p^*+p_{Fn}^2+p_{F\nu_l}^2+2\mu_{\nu_l}\mu_n^*)+(p_{Fl}+p_{Fp}+p_{F\nu_l}-p_{Fn})\\ &\left.\times (p_{Fp}^2+p_{Fl}^2+2\mu_l\mu_p^*)(p_{Fn}^2+p_{F\nu_l}^2+2\mu_{\nu_l}\mu_n^*)\right\}\theta(p_{Fl}+p_{Fp}+p_{F\nu_l}-p_{Fn}). \end{aligned} \tag{A31}$$

In the nonrelativistic limit for nucleons $\mu_N^* \simeq m_N^* \gg p_{FN}$. Therefore

$$\Gamma_{pl\leftrightarrow n\nu} \simeq \frac{G^2T^3}{12\pi^3} m_n^* m_p^* \mu_l \mu_{\nu_l}(p_{Fl}+p_{Fp}+p_{F\nu_l}-p_{Fn})\theta(p_{Fl}+p_{Fp}+p_{F\nu_l}-p_{Fn}), \tag{A32}$$

which coincides with our previous calculation if we assume massless leptons $\mu_l = p_{Fl}$ [see Eq. (24) of Ref. [22]].

In the case where the trapped species in the degenerate matter are antineutrinos rather than neutrinos we have $\mu_{\nu_l}/T \to -\infty$, therefore $I_3 = 0$ and $\Gamma_{pl\leftrightarrow n\nu} = 0$. The logarithm in Eq. (A29) in this case is ω/T and

$$\begin{aligned}\Gamma_{n\to pl\bar{\nu}} &= -\frac{G^2T^3}{48\pi^3}\left\{\frac{(p_{Fl}+p_{Fp})^5-(p_{Fn}-p_{F\bar{\nu}_l})^5}{5}-\frac{(p_{Fl}+p_{Fp})^3-(p_{Fn}-p_{F\bar{\nu}_l})^3}{3}\right.\\ &\times (p_{Fp}^2+p_{Fl}^2+2\mu_l\mu_p^*+p_{Fn}^2+p_{F\bar{\nu}_l}^2-2|\mu_{\nu_l}|\mu_n^*)+(p_{Fl}+p_{Fp}+p_{F\bar{\nu}_l}-p_{Fn})\\ &\left.\times (p_{Fp}^2+p_{Fl}^2+2\mu_l\mu_p^*)(p_{Fn}^2+p_{F\bar{\nu}_l}^2-2|\mu_{\nu_l}|\mu_n^*)\right\}\theta(p_{Fl}+p_{Fp}+p_{F\bar{\nu}_l}-p_{Fn}). \end{aligned} \tag{A33}$$

In Fig. 13 we show the ratios of summed electron Urca rates Γ_e to their low-temperature limit given by Eqs. (A31) and (A33). We see that the exact rates differ significantly from their low-temperature limit typically at $T \geq 10$ MeV, where the deviation between the exact and the approximate rates reaches up to an order of magnitude. Note that the exact rates are mainly larger than their low-temperature limit in neutrino-dominated

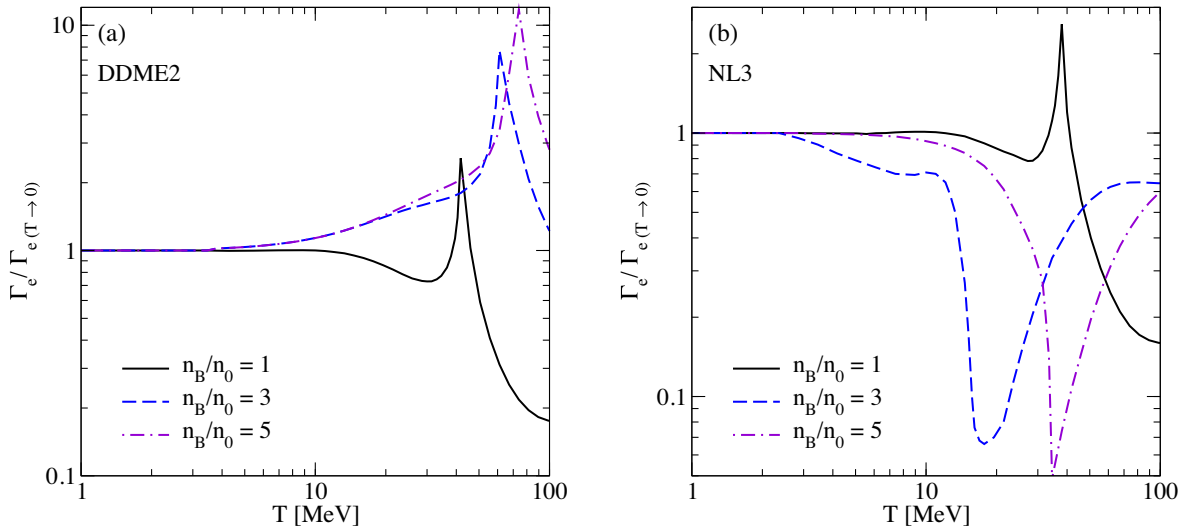

FIG. 13. The ratios of summed electron Urca rates Γ_e to their low-T limit given by (a) Eq. (A31) for model DDME2 and (b) Eq. (A33) model NL3 (b). The analogous ratios for muonic Urca rates are similar and are not shown.

matter and smaller in the antineutrino-dominated matter. The analogous ratios for muonic Urca rates are similar and are not shown.

APPENDIX B: COMPUTATION OF SUSCEPTIBILITIES A_j

To compute the susceptibilities $A_{ij} = (\frac{\partial \mu_i}{\partial n_j})_0$ we use the following formula for the particle densities

$$n_i = \frac{g_i}{2\pi^2}\int_0^\infty p^2 dp[f_i(p) - \bar{f}_i(p)], \tag{B1}$$

where g_i is the spin degeneracy factor, and $f(p)$ and $\bar{f}(p)$ are the distribution functions for particles and antiparticles, respectively. For neutrons, protons, electrons and muons we have $g_i = 2$, and for neutrinos $g_\nu = 1$.

Differentiating the left and right sides of Eq. (B1) with respect to n_j and exploiting the expressions

$$\frac{\partial f_i}{\partial n_j} = -f_i(1-f_i)\frac{1}{T}\left(\frac{m^*}{\sqrt{m^{*2}+p^2}}\frac{\partial m^*}{\partial n_j} - \frac{\partial \mu_i^*}{\partial n_j}\right), \qquad \frac{\partial \bar{f}_i}{\partial n_j} = -\bar{f}_i(1-\bar{f}_i)\frac{1}{T}\left(\frac{m^*}{\sqrt{m^{*2}+p^2}}\frac{\partial m^*}{\partial n_j} + \frac{\partial \mu_i^*}{\partial n_j}\right), \tag{B2}$$

in the case of baryons we obtain

$$\delta_{ij} = -\left(\frac{\partial m^*}{\partial n_j}\right)I_{1i}^- + \left(\frac{\partial \mu_i^*}{\partial n_j}\right)I_{0i}^+, \tag{B3}$$

where

$$I_{qi}^\pm = \frac{1}{\pi^2 T}\int_0^\infty p^2 dp\left(\frac{m^*}{\sqrt{m^{*2}+p^2}}\right)^q [f_i(1-f_i) \pm \bar{f}_i(1-\bar{f}_i)], \quad i = \{n, p\}. \tag{B4}$$

The average values of the meson fields are given by [51]

$$g_\omega \omega_0 = \left(\frac{g_\omega}{m_\omega}\right)^2 (n_n + n_p), \qquad g_\rho \rho_{03} = \frac{1}{2}\left(\frac{g_\rho}{m_\rho}\right)^2 (n_p - n_n), \tag{B5}$$

which gives (recall that $\mu_i^* = \mu_i - g_\omega\omega_0 - g_\rho\rho_{03}I_{3i} - \Sigma_r$)

$$B_{ij} \equiv \frac{\partial \mu_i^*}{\partial n_j} = A_{ij} - \left(\frac{g_\omega}{m_\omega}\right)^2\left[1 + \frac{2n_B}{g_\omega}\frac{\partial g_\omega}{\partial n_B}\right] - I_{3i}\left(\frac{g_\rho}{m_\rho}\right)^2\left[I_{3j} + \frac{n_n - n_p}{n_0}a_\rho\right] - \frac{\partial \Sigma_r}{\partial n_j}. \tag{B6}$$

The scalar field is given by

$$g_\sigma\sigma = m - m^* = -\frac{g_\sigma}{m_\sigma^2}\frac{\partial U(\sigma)}{\partial \sigma} + \frac{1}{\pi^2}\left(\frac{g_\sigma}{m_\sigma}\right)^2 \sum_{i=n,p}\int_0^\infty p^2 dp \frac{m^*}{\sqrt{p^2+m^{*2}}}[f_i(p) + \bar{f}_i(p)], \tag{B7}$$

with $U(\sigma)$ being the self-interaction potential of the scalar field, therefore up to terms $\partial g_\sigma/\partial n_B$ (which are small and can be neglected) we find

$$\begin{aligned}\frac{\partial m^*}{\partial n_j} = {} & \frac{g_\sigma}{m_\sigma^2}\frac{\partial^2 U(\sigma)}{\partial \sigma^2}\frac{\partial \sigma}{\partial n_j} + \left(\frac{g_\sigma}{m_\sigma}\right)^2\left(\frac{\partial m^*}{\partial n_j}\right)(I_{2n}^+ + I_{2p}^+) - \left(\frac{g_\sigma}{m_\sigma}\right)^2(B_{nj}I_{1n}^- + B_{pj}I_{1p}^-) \\ & - \left(\frac{g_\sigma}{m_\sigma}\right)^2\left(\frac{\partial m^*}{\partial n_j}\right)\sum_{i=n,p}\frac{1}{\pi^2}\int_0^\infty p^2 dp \frac{p^2}{(p^2+m^{*2})^{3/2}}[f_i(p) + \bar{f}_i(p)].\end{aligned} \tag{B8}$$

Denoting

$$\tilde{I}_{2i}^+ = I_{2i}^+ - \frac{1}{\pi^2}\int_0^\infty p^2 dp \frac{p^2}{(p^2+m^{*2})^{3/2}}[f_i(p) + \bar{f}_i(p)], \quad i = n, p, \tag{B9}$$

we obtain

$$\frac{\partial m^*}{\partial n_j} = -\frac{(\frac{g_\sigma}{m_\sigma})^2(B_{nj}I_{1n}^- + B_{pj}I_{1p}^-)}{1 - (\frac{g_\sigma}{m_\sigma})^2(\tilde{I}_{2n}^+ + \tilde{I}_{2p}^+) + \frac{1}{m_\sigma^2}\frac{\partial^2 U}{\partial \sigma^2}}. \tag{B10}$$

Substituting this into Eq. (B3) we obtain the following equations for coefficients B_{ij}

$$B_{ij}I^{+}_{0i} - \gamma(B_{nj}I^{-}_{1n} + B_{pj}I^{-}_{1p})I^{-}_{1i} = \delta_{ij}, \tag{B11}$$

where

$$\gamma = \frac{1}{\tilde{I}^{+}_{2n} + \tilde{I}^{+}_{2p} - \beta}, \qquad \beta = \left(\frac{m_\sigma}{g_\sigma}\right)^2 \left(1 + \frac{1}{m_\sigma^2}\frac{\partial^2 U}{\partial \sigma^2}\right). \tag{B12}$$

In the case of $i \neq j$ we find from Eq. (B11)

$$B_{np} = \gamma B_{pp}\frac{I^{-}_{1p}I^{-}_{1n}}{I^{+}_{0n} - \gamma I^{-2}_{1n}}, \qquad B_{pn} = \gamma B_{nn}\frac{I^{-}_{1n}I^{-}_{1p}}{I^{+}_{0p} - \gamma I^{-2}_{1p}}. \tag{B13}$$

Substituting these expressions into Eq. (B11) for $i = j$ we obtain

$$B_{nn} = \frac{I^{+}_{0p} - \gamma I^{-2}_{1p}}{I^{+}_{0n}I^{+}_{0p} - \gamma I^{+}_{0p}I^{-2}_{1n} - \gamma I^{+}_{0n}I^{-2}_{1p}}, \qquad B_{pp} = \frac{I^{+}_{0n} - \gamma I^{-2}_{1n}}{I^{+}_{0n}I^{+}_{0p} - \gamma I^{+}_{0p}I^{-2}_{1n} - \gamma I^{+}_{0n}I^{-2}_{1p}}, \tag{B14}$$

and

$$B_{np} = B_{pn} = \frac{\gamma I^{-}_{1p}I^{-}_{1n}}{I^{+}_{0n}I^{+}_{0p} - \gamma I^{+}_{0p}I^{-2}_{1n} - \gamma I^{+}_{0n}I^{-2}_{1p}}. \tag{B15}$$

Substituting Eqs. (B14) and (B15) in Eq. (B6) and recalling the definitions $A_n = A_{nn} - A_{pn}$, $A_p = A_{pp} - A_{np}$ we obtain

$$A_n = \frac{I^{+}_{0p} - \gamma I^{-}_{1p}(I^{-}_{1p} + I^{-}_{1n})}{I^{+}_{0n}I^{+}_{0p} - \gamma I^{+}_{0p}I^{-2}_{1n} - \gamma I^{+}_{0n}I^{-2}_{1p}} + \left(\frac{g_\rho}{m_\rho}\right)^2 \left(\frac{1}{2} - \frac{n_n - n_p}{n_0}a_\rho\right), \tag{B16}$$

$$A_p = \frac{I^{+}_{0n} - \gamma I^{-}_{1n}(I^{-}_{1p} + I^{-}_{1n})}{I^{+}_{0n}I^{+}_{0p} - \gamma I^{+}_{0p}I^{-2}_{1n} - \gamma I^{+}_{0n}I^{-2}_{1p}} + \left(\frac{g_\rho}{m_\rho}\right)^2 \left(\frac{1}{2} + \frac{n_n - n_p}{n_0}a_\rho\right). \tag{B17}$$

For leptons we have simply

$$A_l = \frac{1}{I^{+}_{0l}}, \qquad A_{\nu_l} = \frac{2}{I^{+}_{0\nu_l}}, \qquad l = \{e, \mu\}. \tag{B18}$$

[1] The LIGO Scientific Collaboration and The Virgo Collaboration, GW170817: Observation of Gravitational Waves from a Binary Neutron Star Inspiral, Phys. Rev. Lett. **119**, 161101 (2017).

[2] R. Abbott, T. D. Abbott, S. Abraham, F. Acernese, K. Ackley *et al.* (LIGO Scientific Collaboration and Virgo Collaboration), GWTC-2: Compact Binary Coalescences Observed by LIGO and Virgo During the First Half of the Third Observing Run, Phys. Rev. X **11**, 021053 (2021).

[3] M. Maggiore, C. Van Den Broeck, N. Bartolo, E. Belgacem, D. Bertacca, M. A. Bizouard *et al.*, Science case for the Einstein telescope, J. Cosmol. Astropart. Phys. 03 (2020) 050.

[4] D. Reitze, R. X. Adhikari, S. Ballmer, B. Barish, L. Barsotti, G. Billingsley *et al.*, Cosmic explorer: The U.S. contribution to gravitational-wave astronomy beyond LIGO, Bull. Am. Astron. Soc. **51**, 35 (2019).

[5] A. Perego, S. Bernuzzi, and D. Radice, Thermodynamics conditions of matter in neutron star mergers, Eur. Phys. J. A **55**, 124 (2019).

[6] M. Hanauske, J. Steinheimer, A. Motornenko, V. Vovchenko, L. Bovard, E. R. Most *et al.*, Neutron star mergers: Probing

the EoS of hot, dense matter by gravitational waves, Particles **2**, 44 (2019).
[7] M. Hanauske, J. Steinheimer, L. Bovard, A. Mukherjee, S. Schramm, K. Takami *et al.*, Concluding remarks: Connecting relativistic heavy ion collisions and neutron star mergers by the equation of state of dense hadron- and quark matter as signalled by gravitational waves, J. Phys. Conf. Ser. **878**, 012031 (2017).
[8] W. Kastaun, R. Ciolfi, A. Endrizzi, and B. Giacomazzo, Structure of stable binary neutron star merger remnants: Role of initial spin, Phys. Rev. D **96**, 043019 (2017).
[9] S. Bernuzzi, D. Radice, C. D. Ott, L. F. Roberts, P. Moesta, and F. Galeazzi, How loud are neutron star mergers?, Phys. Rev. D **94**, 024023 (2016).
[10] F. Foucart, R. Haas, M. D. Duez, E. O'Connor, C. D. Ott, L. Roberts *et al.*, Low mass binary neutron star mergers: Gravitational waves and neutrino emission, Phys. Rev. D **93**, 044019 (2016).
[11] K. Kiuchi, Y. Sekiguchi, K. Kyutoku, and M. Shibata, Gravitational waves, neutrino emissions, and effects of hyperons in binary neutron star mergers, Classical Quantum Gravity **29**, 124003 (2012).
[12] Y. Sekiguchi, K. Kiuchi, K. Kyutoku, and M. Shibata, Gravitational Waves and Neutrino Emission from the Merger of Binary Neutron Stars, Phys. Rev. Lett. **107**, 051102 (2011).
[13] M. Ruiz, R. N. Lang, V. Paschalidis, and S. L. Shapiro, Binary neutron star mergers: A jet engine for short gamma-ray bursts, Astrophys. J. Lett. **824**, L6 (2016).
[14] W. E. East, V. Paschalidis, F. Pretorius, and S. L. Shapiro, Relativistic simulations of eccentric binary neutron star mergers: One-arm spir al instability and effects of neutron star spin, Phys. Rev. D **93**, 024011 (2016).
[15] E. R. Most, L. J. Papenfort, and L. Rezzolla, Beyond second-order convergence in simulations of magnetized binary neutron stars with realistic microphysics, Mon. Not. R. Astron. Soc. **490**, 3588 (2019).
[16] A. Bauswein, N.-U. F. Bastian, D. B. Blaschke, K. Chatziioannou, J. A. Clark, T. Fischer *et al.*, Identifying a First-Order Phase Transition in Neutron-Star Mergers through Gravitational Waves, Phys. Rev. Lett. **122**, 061102 (2019).
[17] L. Baiotti and L. Rezzolla, Binary neutron star mergers: A review of Einstein's richest laboratory, Rep. Prog. Phys. **80**, 096901 (2017).
[18] L. Baiotti, Gravitational waves from neutron star mergers and their relation to the nuclear equation of state, Prog. Part. Nucl. Phys. **109**, 103714 (2019).
[19] J. A. Faber and F. A. Rasio, Binary neutron star mergers, Living Rev. Relativity **15**, 8 (2012).
[20] M. G. Alford, L. Bovard, M. Hanauske, L. Rezzolla, and K. Schwenzer, Viscous Dissipation and Heat Conduction in Binary Neutron-Star Mergers, Phys. Rev. Lett. **120**, 041101 (2018).
[21] M. G. Alford and S. P. Harris, Damping of density oscillations in neutrino-transparent nuclear matter, Phys. Rev. C **100**, 035803 (2019).
[22] M. Alford, A. Harutyunyan, and A. Sedrakian, Bulk viscosity of baryonic matter with trapped neutrinos, Phys. Rev. D **100**, 103021 (2019).
[23] M. G. Alford and A. Haber, Strangeness-changing rates and hyperonic bulk viscosity in neutron star mergers, Phys. Rev. C **103**, 045810 (2021).
[24] M. Alford, A. Harutyunyan, and A. Sedrakian, Bulk viscous damping of density oscillations in neutron star mergers, Particles **3**, 500 (2020).
[25] L. F. Roberts, S. Reddy, and G. Shen, Medium modification of the charged current neutrino opacity and its implications, Phys. Rev. C **86**, 065803 (2012).
[26] M. G. Alford and S. P. Harris, β equilibrium in neutron-star mergers, Phys. Rev. C **98**, 065806 (2018).
[27] E. R. Most, S. P. Harris, C. Plumberg, M. G. Alford, J. Noronha, J. Noronha-Hostler *et al.*, Projecting the likely importance of weak-interaction-driven bulk viscosity in neutron star mergers, Mon. Not. R. Astron. Soc., stab2793 (2021), https://doi.org/10.1093/mnras/stab2793.
[28] R. F. Sawyer and A. Soni, Transport of neutrinos in hot neutron-star matter, Astrophys. J. **230**, 859 (1979).
[29] R. F. Sawyer, Damping of neutron star pulsations by weak interaction processes, Astrophys. J. **237**, 187 (1980).
[30] R. F. Sawyer, Bulk viscosity of hot neutron-star matter and the maximum rotation rates of neutron stars, Phys. Rev. D **39**, 3804 (1989).
[31] P. Haensel and R. Schaeffer, Bulk viscosity of hot-neutron-star matter from direct URCA processes, Phys. Rev. D **45**, 4708 (1992).
[32] P. Haensel, K. P. Levenfish, and D. G. Yakovlev, Bulk viscosity in superfluid neutron star cores. I. Direct Urca processes in npemu matter, Astron. Astrophys. **357**, 1157 (2000).
[33] P. Haensel, K. P. Levenfish, and D. G. Yakovlev, Bulk viscosity in superfluid neutron star cores. II. Modified Urca processes in npe mu matter, Astron. Astrophys. **372**, 130 (2001).
[34] H. Dong, N. Su, and Q. Wang, Bulk viscosity in nuclear and quark matter, J. Phys. G Nucl. Phys. **34**, S643 (2007).
[35] M. G. Alford, S. Mahmoodifar, and K. Schwenzer, Large amplitude behavior of the bulk viscosity of dense matter, J. Phys. G Nucl. Phys. **37**, 125202 (2010).
[36] E. E. Kolomeitsev and D. N. Voskresensky, Viscosity of neutron star matter and r-modes in rotating pulsars, Phys. Rev. C **91**, 025805 (2015).
[37] M. G. Alford and G. Good, Leptonic contribution to the bulk viscosity of nuclear matter, Phys. Rev. C **82**, 055805 (2010).
[38] G. A. Lalazissis, T. Nikšić, and D. Vretenar, and P. Ring, New relativistic mean-field interaction with density-dependent meson-nucleon couplings, Phys. Rev. C **71**, 024312 (2005).
[39] G. A. Lalazissis, J. König, and P. Ring, New parametrization for the Lagrangian density of relativistic mean field theory, Phys. Rev. C **55**, 540 (1997).
[40] M. Prakash, I. Bombaci, M. Prakash, P. J. Ellis, J. M. Lattimer, and R. Knorren, Composition and structure of protoneutron stars, Phys. Rep. **280**, 1 (1997).
[41] G. Malfatti, M. G. Orsaria, G. A. Contrera, F. Weber, and I. F. Ranea-Sandoval, Hot quark matter and (proto-) neutron stars, Phys. Rev. C **100**, 015803 (2019).
[42] F. Weber, D. Farrell, W. M. Spinella, G. Malfatti, M. G. Orsaria, G. A. Contrera *et al.*, Phases of hadron-quark matter in (proto) neutron stars, Universe **5**, 169 (2019).
[43] G. Guo, G. Martínez-Pinedo, A. Lohs, and T. Fischer, Charged-current muonic reactions in core-collapse supernovae, Phys. Rev. D **102**, 023037 (2020).

[44] T. Fischer, G. Guo, G. Martínez-Pinedo, M. Liebendörfer, and A. Mezzacappa, Muonization of supernova matter, Phys. Rev. D **102**, 123001 (2020).

[45] W. Greiner and B. Müller, *Gauge Theory of Weak Interactions*, Physics and Astronomy Online Library (Springer, New York, 2000).

[46] N. K. Glendenning, *Compact Stars: Nuclear Physics, Particle Physics, and General Relativity* (Springer, New York, N.Y., 2000).

[47] F. Weber, *Pulsars as Astrophysical Laboratories for Nuclear and Particle Physics* (Institute of Physics, Bristol, U.K., 1999).

[48] S. Typel and H. H. Wolter, Relativistic mean field calculations with density-dependent meson-nucleon coupling, Nucl. Phys. **A656**, 331 (1999).

[49] P. B. Jones, Bulk viscosity of neutron-star matter, Phys. Rev. D **64**, 084003 (2001).

[50] Note that the temperature is assumed to be constant because, as argued in the Sec. I, we assume that the thermal equilibration rate is much larger than the chemical equilibration rate.

[51] D. Chatterjee and D. Bandyopadhyay, Bulk viscosity in kaon condensed matter, Phys. Rev. D **75**, 123006 (2007).